

Control of a Chaotic Double Pendulum Model for a Ship Mounted Crane

Tseng-Hsing Hsu

Dissertation submitted to the Faculty of the
Virginia Polytechnic Institute and State University
in partial fulfillment of the requirements for the degree of

Doctor of Philosophy
in
Engineering Mechanics

Scott L. Hendricks, Chair

William J. Floyd

Ronald D. Kriz

Dean T. Mook

Mahendra P. Singh

February 22, 2000

Blacksburg, Virginia

Control of a Chaotic Double Pendulum Model for a Ship Mounted Crane

Tseng-Hsing Hsu

(ABSTRACT)

An extension of the original Ott-Grebog-Yorke control scheme is used on a simple double pendulum. The base point of the double pendulum moves in both horizontal and vertical directions which leads to rather complicated behavior. A delay coordinate is used to reconstruct the attractor. The required dimension is determined by the False Nearest Neighbor analysis. A newly developed Fixed Point Transformation method is used to identify the unstable periodic orbit (UPO). Two different system parameters are used to control the motion. Minimum parameter constraints are studied. The use of discrete values for parameter changes is also investigated. Based on these investigation, a new on-off control scheme is proposed to simplify the implementation of the controller and minimize the delay in applying the control.

Acknowledgments

I wish to express my sincere appreciation to my advisor, Dr. Scott L. Hendricks, for his teaching, guidance, and support throughout the course of this research. I would also like to thank the committee members, Dr. William J. Floyd, Dr. Ronald D. Kriz, Dr. Dean T. Mook, and Dr. Mahendra P. Singh.

Last but not least, I wish to thank my parents. Without their love and support, it will be impossible for me to finish my study. I dedicate this work to them.

Contents

1	Introduction	1
1.1	Motivation	1
1.2	Outline	2
2	Literature Review	4
2.1	Chaos	4
2.2	Control of Chaos	7
2.3	Software Tools	9
3	Formulation	10
3.1	Nonlinear Equations of Motion	10
3.2	Determining the Dimension Required for the Reconstructed Attractor	15
3.3	Extracting the Unstable Periodic Orbit (UPO) from Data Sets	17
3.4	Control	19
4	Numerical Result	26
4.1	Chaos	26

4.2	Dimension of Embedding	33
4.3	Determining the Fixed Point	36
4.4	Control Using Horizontal Oscillation of the Base Point as the Control Parameter	38
4.5	Control Using Torque on the Lower Part of the Double Pendulum as the Control Parameter	48
4.6	The On-Off Control	57
5	Conclusion and Future Work	63
5.1	Conclusion	63
5.2	Future Work	64
	Bibliography	66
	Appendix	
A	Equations of Motion in First Order Form	73
B	Validation of the Fixed Point Transformation Method	75
B.1	Logistic Map	75
B.2	Hénon Map	76

List of Figures

3.1	The setup of the system	11
3.2	Geometric Interpretation of the Transformation in One Dimension for the Case $\mathbf{R} = 0$	18
3.3	Illustration of the OGY Control Procedure (from Ditto et al., 1990 [12]) . . .	21
4.1	θ_1 vs θ_2	27
4.2	$\dot{\theta}_1$ vs $\dot{\theta}_2$	28
4.3	θ_1 vs $\dot{\theta}_1$	29
4.4	θ_2 vs $\dot{\theta}_2$	30
4.5	FFTs of θ_1 , θ_2 , $\dot{\theta}_1$, and $\dot{\theta}_2$	31
4.6	$\dot{\theta}_2(n)$ vs $\dot{\theta}_2(n + 1)$	32
4.7	Estimation of the Maximum Lyapunov Exponent	34
4.8	The Result of the False Nearest Neighbor Analysis	35
4.9	Histogram of the Transformed Data Set	37
4.10	Control of the System with Only Maximum Restriction on the Control Para- meter	40
4.11	Scatter Plot of the Control Parameter at Each Iteration	41

4.12 Control with Both Minimum and Maximum Restriction on the Control Parameter	42
4.13 Scatter Plot of the Control Parameter at Each Iteration	43
4.14 Control with Maximum and Discrete Value Restriction on the Control Parameter	44
4.15 Scatter Plot of the Control Parameter at Each Iteration	45
4.16 Average Values and Standard Deviations for Different Minimum Value for the Control Parameter Change (Top) and Different Step Size for the Control Parameter Change (Bottom)	47
4.17 Control of the System with Only Maximum Restriction on the Control Parameter	49
4.18 Scatter Plot of the Control Parameter at Each Iteration	50
4.19 Control with Both Minimum and Maximum Restriction on the Control Parameter	51
4.20 Scatter Plot of the Control Parameter at Each Iteration	52
4.21 Control with Maximum and Discrete Value Restriction on the Control Parameter	53
4.22 Scatter Plot of the Control Parameter at Each Iteration	54
4.23 Average Values and Standard Deviations for Different Minimum Value for the Control Parameter Change (Top) and Different Step Size for the Control Parameter Change (Bottom)	56
4.24 Control Using the On-Off Approach	58
4.25 Scatter Plot of the Control Parameter at Each Iteration	59
4.26 θ_1 at Each Iteration	60
4.27 θ_2 at Each Iteration	61

4.28	$\dot{\theta}_1$ at Each Iteration	62
B.1	1000 Iterations of the Logistic Map	77
B.2	The Histogram of the Tranformed Logistic Map Data Set	78
B.3	5000 Iterations of the Hénon Map	79
B.4	False Nearest Neighbor Analysis for Hénon Map	80
B.5	The Histogram of the Tranformed Data Set for Hénon Map	81

List of Tables

4.1	The Average Value and Standard Deviation of the Observable	46
4.2	The Average Value and Standard Deviation of the Observable	55

Chapter 1

Introduction

1.1 Motivation

The study of chaos leads to new understanding of nonlinear systems. Currently researchers try to utilize various characteristics of nonlinear systems to their advantage instead of avoiding them. The Ott-Grebogy-Yorke (OGY) control scheme [40] is one method used to control chaotic behavior.

What separates the OGY scheme from the others is its versatility. The other advantage of this scheme is that exact knowledge of the system is not required. Researchers have used the scheme on various systems with good success. The range of application includes biology (Garfinkel et al. [17]), electronics (Hunt [24]), and lasers (Gills et al. [18], Reyl et al. [50]). One area that has not received much attention is the mechanical system. Except for studies on a magnetoelastic ribbon by Ditto et al. [12], a kicked double rotor [5], and a simple pendulum [61], there is hardly anything done in this area. A good candidate for research in this direction is the double pendulum. On one hand, the system is simple yet exhibits chaos under certain excitations. On the other hand, the system can be used as a model for the ship-mounted crane. It is possible that the research can eventually lead to practical use.

The ship mounted crane is a complicated system. The heave and roll of the ship in the sea have a great effect on the pendulation. The effects of the heave and roll can be even worse when the frequencies match those of the parametric or primary resonance of the crane. Under these condition, even a small heave or roll will have a large effect on the pendulation. The Maryland rigging proposed by Grebogy et al. [19] and the passive control scheme by Lacarbonara [29] perform well under normal non-chaotic conditions. Both of these schemes work on a system that can be modeled as a double pendulum. If the OGY control scheme can be used on the double pendulum, it can be beneficial in two respects. First, though not feasible to use it under all conditions, it can certainly be used to supplement the previously mentioned control schemes and to extend the range of operations to control chaotic motion. Second, OGY only requires small changes in the system parameters. The two control schemes mentioned already have some mechanisms built in so that certain system parameters are available to be used in the OGY control scheme. That is to say no system alteration is required. All that is needed is to add a second control scheme to the controller so that the OGY scheme kicks in when a pre-set condition is met.

It is the purpose of the proposed study to investigate the effectiveness and feasibility of applying the OGY control scheme to a mechanical system, specifically a double pendulum with a horizontally and vertically oscillating base point. By establishing the effectiveness and feasibility of the OGY scheme on the double pendulum, it can then give indications if it is possible to implement this control scheme on ship-mounted cranes.

1.2 Outline

This dissertation is organized as follows:

- Chapter 2 is the literature review. A short review of the development of chaos is presented. The OGY control scheme and pertinent papers are listed along with some different schemes. Various methods to analyze the experimental data are reviewed.

- In chapter 3, the equations of motion for the double pendulum under study are derived. The frequencies of the excitation used in the study are calculated using a multiple-scale perturbation method. The algorithm for extracting unstable periodic orbits and control are also explained in this chapter.
- Chapter 4 presents the results of the control.
- Chapter 5 is the conclusion with suggestions for future work.

Chapter 2

Literature Review

2.1 Chaos

The study of chaotic behavior in a deterministic system began as early as the turn of this century. Although Poincaré [46] did not specifically call the behavior chaos, he realized that he could not predict the behavior of three gravitationally attracting bodies despite knowing the exact equations that describe their motion. In the decades after Poincaré published his paper, progress has been made in the qualitative aspects of nonlinear systems. On the quantitative side, approximate schemes were devised to tackle weakly nonlinear system with success. See the book of Nayfeh and Mook [37] for more references. However, these schemes failed to address quantitatively the problem of general nonlinear systems.

Things changed dramatically with the introduction of the computer. All of a sudden scientists were given the tool to numerically study previously intractable nonlinear systems. With the ability to quantitatively study nonlinear systems comes the unexpected conflict with long held beliefs obtained from the study of linear systems. In 1963, while trying to simulate the behavior of weather pattern, Lorenz [32] discovered that a small deviation in initial conditions can lead to dramatically different results in some nonlinear systems. After

Lorenz's discovery, a flood of research was done on finding chaos in various nonlinear systems. Holmes [22] used the Duffing-type equation to study the behavior of a buckled beam. And he showed that chaos is possible from the result obtained from an analog computer. Moon and Holmes [34] observed chaotic behavior from a magnetoelastic buckled beam experiment. Ueda [63] discovered chaotic behavior in a nonlinear electric circuit. In 1981, McLaughlin [33] numerically studied the chaotic behavior of a parametrically forced pendulum. Most introductory books on nonlinear dynamics have a list of chaos observed in various systems (e.g. Moon [35] and Rasband [49]). The books by Devaney [10] (for discrete systems) and by Guckenheimer and Holmes [20] (for continuous systems) offer excellent introductions to the study of chaos.

While chaos is characterized as a phenomenon that is sensitive to minor differences in initial conditions, the quantitative way to describe it lies in the exponential separation of two initially close orbits. The measure of how fast these two trajectories separate from each other is the Lyapunov exponent. If a system has a positive Lyapunov exponent, it is chaotic. When the equations for the system under study are known, it is relatively easy to calculate the exponent. But in the real world, most data sets are obtained from systems whose equations are unknown. It is then necessary to develop a way to calculate the Lyapunov exponents from a data set without the benefit of knowing the underlying equations for the system. Wolf [64] is one of the first to propose an algorithm to do this. In the same paper, he also provided a way to calculate Lyapunov exponents from equations for the system. Later, Sano and Sawada [54] as well as Eckmann et al. [15] proposed ways to calculate the whole Lyapunov exponent spectrum from a data set. The problem with these algorithms is that they need a good data set. That is to say the data set should be big enough so that each point has a close enough neighboring point. And a good estimation of the embedding is essential for these algorithms to have an accurate estimation of the exponents. More recently, Rosenstein, Collins, and de Luca [52] and Kantz [25] independently proposed similar algorithms to calculate the maximum Lyapunov exponent.

When the system under study is simple or the equations of motion are known, it is easy

to determine the actual dimension of the system. In reality, most experiments can only observe a small number of variables instead of the whole system. In 1980, Packard et al. [42] proposed the idea of using time-delay coordinates to reconstruct a phase portrait from a time series. Takens [62] (reprinted in Ott et al. [41]) independently published a mathematical proof of the validity of using time-delay coordinates to reconstruct the phase portrait in 1981. A more accessible account of the time-delay coordinate embedding can be found in the book by Ott et al. [39]. It is a significant step in the study of chaos. Armed with this technique, researchers can now study a nonlinear system even when the exact equations of motion are unknown.

Takens [62] also showed that if d_A is the dimension of the attractor, then a reconstructed attractor using a time-delay coordinate with dimension d_E can retain all the topological properties of the original attractor if $d_E > 2d_A$. This is a sufficient condition and can be used to determine an upper bound on the dimension. It was still necessary to determine the minimum dimension required to properly represent the original attractor using time-delay coordinates. As pointed out in the paper by Kennel, Brown, and Abarbanel [27], the strange attractor of the Lorenz equations has a box counting dimension $d_A = 2.06$. According to the theorem by Takens, the embedded dimension $d_E = 5$ will represent the attractor for sure. But as it happens, $d_E = 3$ will also do it if the coordinate $x(t)$ is used as the observable. In the same paper, Kennel, Brown, and Abarbanel proposed the idea of using False Nearest Neighbors (FNN) to determine the minimum dimension required. Abarbanel et al. later published a review paper [2] that gave a more in depth look at the analysis of observed data in general. More recently, the books by Abarbanel [1] and Kantz and Schreiber [26] provide systematic approaches to experimental time-series analysis.

2.2 Control of Chaos

After much research where chaos was found in various nonlinear systems, researchers started to think about using this newly found phenomenon in applications. In 1989, Hübler and Lüscher [23] proposed a non-feedback control scheme. Their scheme does control; however their scheme usually requires a large perturbation to the system and a knowledge of the model equations for the system.

In 1990, Ott, Grebogy, and Yorke [40] proposed a new feedback-control scheme. It is usually referred to as the OGY control scheme. Their scheme is different from that of Hübler and Lüscher. It is based on the observation that there are unstable periodic orbits embedded in the strange attractor. By giving a suitable feedback, it is possible to nudge the system onto the stable manifold of a chosen unstable periodic orbit and thus converge to that orbit. This feedback scheme has the advantage that it requires only a small perturbation of accessible system parameters, it can control more than one mode and it does not require knowledge of the exact equations of the system. But there are some shortcomings as well. Most notably, the transient before control is established is usually long and the scheme is not robust with respect to noise when the positive eigenvalue of the unstable periodic orbit is large.

The first application of OGY in an experimental setup came in 1990. Ditto et al. [12] used it on a magnetoelastic ribbon. With the initial success of the feedback control scheme, a flood of research was done on controlling chaos. Romeiras et al. [51] applied the scheme to a periodically impulsively kicked mechanical system. Hunt [24] modified the OGY algorithm and developed an “occasional proportional feedback” (OPF) control scheme. In 1992, Dressler and Nitsche [14] modified the OGY scheme to obtain better control when time delay coordinates are used. Garfinkel et al. [17] used the scheme to stabilize cardiac arrhythmias in rabbit ventricles. Roy et al. [53] used it to control a multimode laser. Petrov [45] applied the OGY scheme to a chemical reaction. Pyragas [47] proposed a continuous feedback-control scheme to overcome some of the shortcomings of the OGY scheme in 1992. The Pyragas scheme was used in an experimental setup in 1993 [48]. In 1992, Shinbrot,

Grebowi, and Yorke [57] developed a method to target the chaotic orbit toward a desired state in a much shorter time than the natural evolution of the system. Later Kostelich et al. [28] proposed a procedure to do higher dimensional targeting. Lai, Ding, and Grebowi [30] extended the OGY method so that it can be used to control Hamiltonian systems which may have complex eigenvalues. Alsing, Gavrelides, and Kovanis [3] trained a neural network to apply OGY on chaotic systems. In a 1994 paper, Alvarez-Ramírez [4] used a non-linear feedback scheme to shorten the transient time. Barreto and Grebowi [7] extended the OGY scheme to use multiple available system parameters to shorten the transient time. In 1997, Boccaletti et al. [8] developed an adaptive targeting scheme. Shroer et al. [55] proposed the idea of using a targeting scheme to control a ship-mounted crane in 1997. But there have been no follow up papers that actually applied this scheme to the ship-mounted crane. The review article of Shinbrot [56], although a little outdated, has a more comprehensive account of the progress of the control scheme up to 1995.

In order to use the OGY control scheme, the unstable periodic orbit embedded in the strange attractor has to be identified. The straightforward way to do this is to look at the recurrent neighborhood. The idea is that if an orbit started at x_0 comes back to a predefined neighborhood of x_0 after time T , then x_0 has a periodic orbit with period T (see [31] and [16]) The method requires a long data set to be able to more accurately determine the Unstable Periodic Orbit (UPO). It is also important to determine an optimal neighborhood size. In 1996, So et al. [59] proposed to utilize a transformation on the data such that the transformed data set will be concentrated around the UPO. It is then possible to identify the location of the UPO by taking a histogram of the transformed data. The original paper deals with finding the UPO of period 1. In theory it can be applied to finding UPO of period n by taking every n -th point in the original data set. The straightforward extension will not work well in the presence of noise or large Lyapunov exponents. In a later paper, So et al. [58] extended the method to be able to identify higher period UPO. So et al. [60] used this method to locate UPO in data obtained from neuronal systems. Later, Bak et al. [6] identified UPO in the data from nuclear-fusion experimentation by using the recurrent-neighborhood method as

well as So's method.

2.3 Software Tools

A large part of the studies of nonlinear data depend on the use of a computer. Over the years, many programs have been developed by serious researchers and hobbyists. Some of these programs plot strange attractors, and some of them can only be used as teaching tools because of their limited scope. But there are also software tools available that are useful enough to be used in research. One such program is the AUTO package [13] which is used to study bifurcations. Wolf made available a program to calculate the Lyapunov exponents using the algorithm proposed in his paper [64]. The TISEAN package from Hegger, Kantz, and Schreiber [21] can be used to study the optimal time-delay, proper embedded dimension, Lyapunov exponents etc. This paper also describes the algorithm used in the package and source codes are distributed along with the execution files. The Nonlinear Dynamics Toolbox (NDT) from Georgia Tech is quite new but versatile. The drawback of NDT is that it is only available as execution files without source code. It is then impossible to figure out the algorithm used without a thorough manual and it is also impossible to modify the code to fit the system under study. Some software eventually becomes commercial. The INSITE package is an implementation of the algorithm presented by Parker and Chua ([43] and [44]). The implementation of the algorithm in Abarbanel's book [1] can be obtained through a license. A good starting point for the various software available is the Nonlinear Science FAQ (Frequently asked Questions) on the World Wide Web (<http://amath.colorado.edu/appm/faculty/jdm/faq.html>). Whenever one of these software package is used in this research, it is identified.

Chapter 3

Formulation

In this chapter, the equations of motion for the system under study are derived. The natural frequencies of the linearized free motion are calculated. The method of multiple scales [36] is then used to determine the frequency of the excitation which will produce the maximum effect. The false-nearest-neighbor procedure is discussed and used later to determine the dimension required to properly reconstruct the attractor using time-delay coordinate embedding. Methods to extract UPO from a data set are introduced and an algorithm of the high-dimensional OGY control is explained.

3.1 Nonlinear Equations of Motion

The system under study is illustrated in figure 3.1. The motion of the base point is:

$$\begin{aligned}x &= A \cos \omega_1 t \\y &= B \cos \omega_2 t .\end{aligned}\tag{3.1}$$

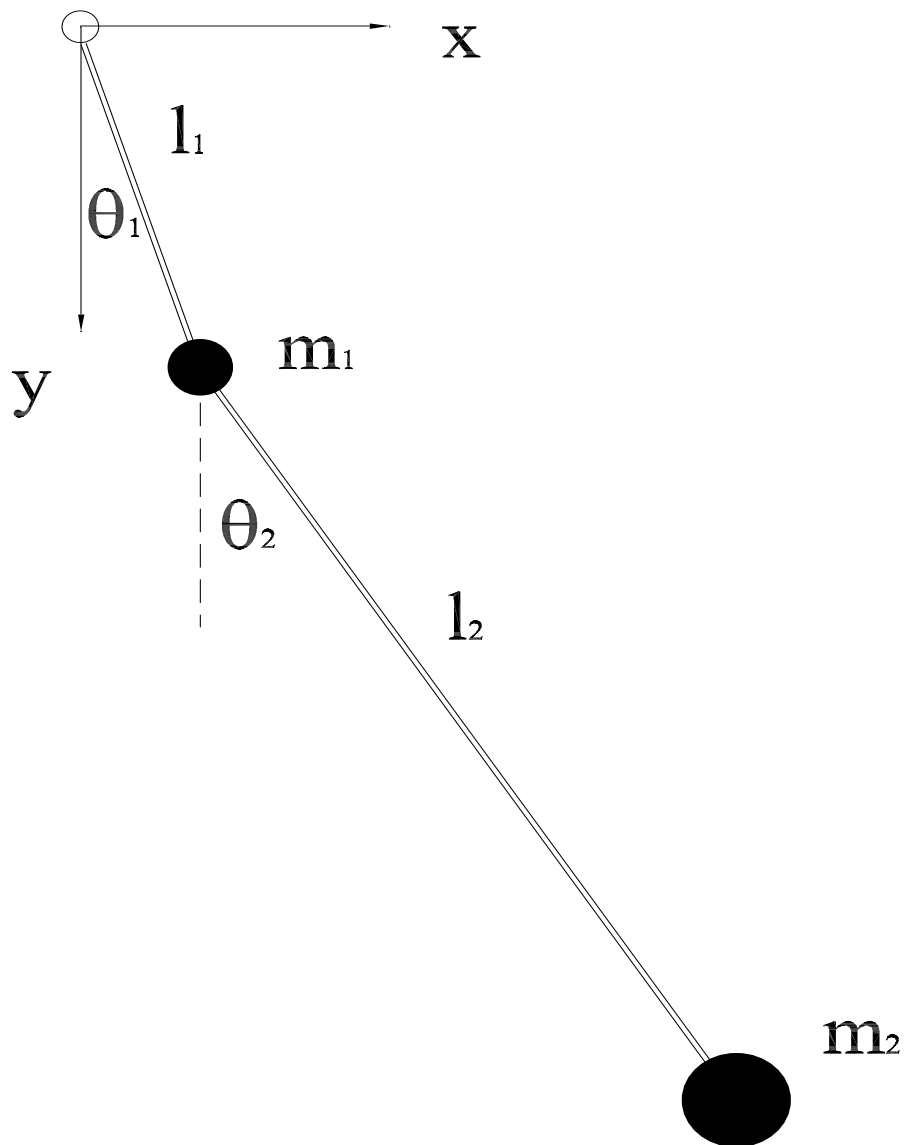


Figure 3.1: The setup of the system

The coordinates of the masses are therefore:

$$\begin{aligned}
x_1 &= A \cos \omega_1 t + l_1 \sin \theta_1 \\
y_1 &= B \cos \omega_2 t + l_1 \cos \theta_1 \\
x_2 &= A \cos \omega_1 t + l_1 \sin \theta_1 + l_2 \sin \theta_2 \\
y_2 &= B \cos \omega_2 t + l_1 \cos \theta_1 + l_2 \cos \theta_2
\end{aligned} \tag{3.2}$$

and the velocities are:

$$\begin{aligned}
\dot{x}_1 &= -A\omega_1 \sin \omega_1 t + l_1 \cos \theta_1 \dot{\theta}_1 \\
\dot{y}_1 &= -B\omega_2 \sin \omega_2 t - l_1 \sin \theta_1 \dot{\theta}_1 \\
\dot{x}_2 &= -A\omega_1 \sin \omega_1 t + l_1 \cos \theta_1 \dot{\theta}_1 + l_2 \cos \theta_2 \dot{\theta}_2 \\
\dot{y}_2 &= -B\omega_2 \sin \omega_2 t - l_1 \sin \theta_1 \dot{\theta}_1 - l_2 \sin \theta_2 \dot{\theta}_2 .
\end{aligned} \tag{3.3}$$

The Lagrangian of the system is:

$$\begin{aligned}
\mathcal{L} &= \frac{m_1 + m_2}{2} (A^2 \omega_1^2 \sin^2 \omega_1 t + B^2 \omega_2^2 \sin^2 \omega_2 t) \\
&+ (m_1 + m_2) l_1 \dot{\theta}_1 (B\omega_2 \sin \omega_2 t \sin \theta_1 - A\omega_1 \sin \omega_1 t \cos \theta_1) \\
&+ m_2 l_2 \dot{\theta}_2 (B\omega_2 \sin \omega_2 t \sin \theta_2 - A\omega_1 \sin \omega_1 t \cos \theta_2) \\
&+ \frac{m_1 + m_2}{2} l_1^2 \dot{\theta}_1^2 + \frac{m_2}{2} l_2^2 \dot{\theta}_2^2 + m_2 l_1 l_2 \dot{\theta}_1 \dot{\theta}_2 (\cos \theta_1 \cos \theta_2 + \sin \theta_1 \sin \theta_2) \\
&+ (m_1 + m_2) g (B \cos \omega_2 t + l_1 \cos \theta_1) + m_2 g l_2 \cos \theta_2 .
\end{aligned} \tag{3.4}$$

The equations of motion can be derived from equation 3.4 by using

$$\frac{d}{dt} \left(\frac{\partial \mathcal{L}}{\partial \dot{\theta}_i} \right) - \frac{\partial \mathcal{L}}{\partial \theta_i} = 0 \tag{3.5}$$

where $i = 1, 2$. The equations of motion obtained are the following:

$$\begin{aligned}
(m_1 + m_2) l_1^2 \ddot{\theta}_1 + (m_1 + m_2) l_1 (B\omega_2^2 \cos \omega_2 t \sin \theta_1 - A\omega_1^2 \cos \omega_1 t \cos \theta_1) \\
+ m_2 l_1 l_2 \ddot{\theta}_2 \cos(\theta_1 - \theta_2) + m_2 \sin(\theta_1 - \theta_2) \dot{\theta}_2^2 + (m_1 + m_2) g l_1 \sin \theta_1 = 0
\end{aligned} \tag{3.6}$$

$$\begin{aligned}
m_2 l_1 l_2 \cos(\theta_1 - \theta_2) \ddot{\theta}_1 + m_2 l_2 (B\omega_2^2 \cos \omega_2 t \sin \theta_2 - A\omega_1^2 \cos \omega_1 t \cos \theta_2) + m_2 l_2^2 \ddot{\theta}_2 \\
- m_2 l_1 l_2 \sin(\theta_1 - \theta_2) \dot{\theta}_1^2 + m_2 g l_2 \sin \theta_2 = 0 .
\end{aligned} \tag{3.7}$$

Let the friction at the base point be proportional to $\dot{\theta}_1$ and the friction in the middle be proportional to $\dot{\theta}_2 - \dot{\theta}_1$. Putting the effect of friction into equations 3.6 and 3.7, the final equations of motion become:

$$(m_1 + m_2)l_1^2\ddot{\theta}_1 + (m_1 + m_2)l_1(B\omega_2^2 \cos \omega_2 t \sin \theta_1 - A\omega_1^2 \cos \omega_1 t \cos \theta_1) + \alpha_1\dot{\theta}_1 + m_2l_1l_2\ddot{\theta}_2 \cos(\theta_1 - \theta_2) + m_2 \sin(\theta_1 - \theta_2)\dot{\theta}_2^2 + (m_1 + m_2)gl_1 \sin \theta_1 = 0 \quad (3.8)$$

$$m_2l_1l_2 \cos(\theta_1 - \theta_2)\ddot{\theta}_1 + m_2l_2(B\omega_2^2 \cos \omega_2 t \sin \theta_2 - A\omega_1^2 \cos \omega_1 t \cos \theta_2) + m_2l_2^2\ddot{\theta}_2 + \alpha_2(\dot{\theta}_2 - \dot{\theta}_1) - m_2l_1l_2 \sin(\theta_1 - \theta_2)\dot{\theta}_1^2 + m_2gl_2 \sin \theta_2 = 0 \quad (3.9)$$

where α_1 and α_2 are the coefficients of friction at the corresponding joints. Let

$$\begin{aligned} \omega &= \sqrt{\frac{g}{l_2}} & \tau &= \omega t \\ \frac{l_1}{l_2} &= l & \frac{m_2}{(m_1 + m_2)} &= m \\ \frac{\omega_1}{\omega} &= \tilde{\omega}_1 & \frac{\omega_2}{\omega} &= \tilde{\omega}_2 \\ \frac{\alpha_1}{m_2l_2^2\omega} &= \mu_1 & \frac{\alpha_2}{m_2l_2^2\omega} &= \mu_2 \\ \frac{A}{l_2} &= \delta & \frac{B}{l_2} &= \eta \\ \frac{d}{d\tau}(\cdot) &= (\cdot)' . \end{aligned} \quad (3.10)$$

Substituting equations 3.10 into equations 3.8 and 3.9, the non-dimensional equations of motion are

$$\theta_1'' + \frac{m}{l} \cos(\theta_1 - \theta_2)\theta_2'' + \mu_1 \frac{m}{l^2}\theta_1' + \frac{m}{l} \sin(\theta_1 - \theta_2)(\theta_2')^2 + \frac{1}{l} \sin \theta_1 + \frac{\eta}{l}\tilde{\omega}_2^2 \cos \tilde{\omega}_2 \tau \sin \theta_1 - \frac{\delta}{l}\tilde{\omega}_1^2 \cos \tilde{\omega}_1 \tau \cos \theta_1 = 0 \quad (3.11)$$

$$l \cos(\theta_1 - \theta_2)\theta_1'' + \theta_2'' + \mu_2(\theta_2' - \theta_1') - l \sin(\theta_1 - \theta_2)(\theta_1')^2 + \sin \theta_2 + \eta\tilde{\omega}_2^2 \cos \tilde{\omega}_2 \tau \sin \theta_2 - \delta\tilde{\omega}_1^2 \cos \tilde{\omega}_1 \tau \cos \theta_2 = 0 . \quad (3.12)$$

The undamped, unforced linear natural frequencies of the system are obtained by first removing the damping and excitation from equations 3.11, 3.12 and then linearizing them around 0. The resulting equations of motion are:

$$\begin{aligned}\theta_1'' + \frac{m}{l}\theta_2'' + \frac{1}{l}\theta_1 &= 0 \\ l\theta_1'' + \theta_2'' + \theta_2 &= 0.\end{aligned}\tag{3.13}$$

From equations 3.13, the natural frequencies of the system are calculated as

$$\begin{aligned}\omega_{n1} &= \sqrt{\frac{1+l-\sqrt{1-2l+l^2+4lm}}{2l(1-m)}} \\ \omega_{n2} &= \sqrt{\frac{1+l+\sqrt{1-2l+l^2+4lm}}{2l(1-m)}}.\end{aligned}\tag{3.14}$$

After the natural frequencies of the linearized free-vibration system are identified, it is then possible to determine the frequencies of the excitation that will produce the maximum effect on the system. In order to do so, a perturbation method (specifically, the method of multiple scales) is used to determine these frequencies. The bookkeeping parameter ϵ , which is a measure of the amplitude of the motion, is introduced. For the excitation and damping to show up in the order ϵ^2 , it is necessary to do the following substitution:

$$\begin{aligned}\mu_1 &= \epsilon\mu_1 & \mu_2 &= \epsilon\mu_2 \\ \delta &= \epsilon^2\delta & \eta &= \epsilon\eta \\ \theta_1 &= \epsilon\theta_{11} + \epsilon^2\theta_{12} + \dots \\ \theta_2 &= \epsilon\theta_{21} + \epsilon^2\theta_{22} + \dots \\ \tau &= T_0 + \epsilon T_1 + \epsilon^2 T_2 + \dots.\end{aligned}\tag{3.15}$$

Equations 3.15 are substituted into the original non-dimensional equations of motion (equations 3.11) and the notation $D_i^m(\cdot) = \frac{\partial^{(m)}}{\partial T_i^m}(\cdot)$ is used. The terms are then collected according to the order of ϵ . The resulting equations are:

Order ϵ :

$$\begin{aligned}D_0^2\theta_{11} + \frac{m}{l}D_0^2\theta_{21} + \frac{\theta_{11}}{l} &= 0 \\ lD_0^2\theta_{11} + D_0^2\theta_{21} + \theta_{21} &= 0\end{aligned}\tag{3.16}$$

Order ϵ^2 :

$$\begin{aligned}
D_0^2\theta_{12} + \frac{m}{l}D_0^2\theta_{22} + \frac{\theta_{12}}{l} &= -2D_0D_1\theta_{11} - \frac{2m}{l}D_0D_1\theta_{21} - \frac{m\mu_1}{l^2}D_0\theta_{11} \\
&\quad - \frac{\eta\tilde{\omega}_2^2}{l}\theta_{11}\cos\tilde{\omega}_2\tau + \frac{\delta\tilde{\omega}_1^2}{l}\cos\tilde{\omega}_1\tau \\
lD_0^2\theta_{12} + D_0^2\theta_{22} + \theta_{22} &= -2lD_0D_1\theta_{11} - 2D_0D_1\theta_{21} - \mu_2(D_0\theta_{11} - D_0\theta_{21}) \\
&\quad - \eta\tilde{\omega}_2^2\theta_{21}\cos\tilde{\omega}_2\tau + \delta\tilde{\omega}_1^2\cos\tilde{\omega}_1\tau.
\end{aligned} \tag{3.17}$$

The order- ϵ equations are just the equations for the linearized free-vibration system. The $\tilde{\omega}_1$ and $\tilde{\omega}_2$ are chosen such that they will produce secular terms in the order ϵ^2 equations. From equations 3.16, θ_{11} and θ_{21} can be written as

$$\begin{aligned}
\theta_{11}(T_0, T_1, \dots) &= A(T_1, T_2, \dots)\exp(i\omega_{n1}T_0) + B(T_1, T_2, \dots)\exp(i\omega_{n2}T_0) + C.C. \\
\theta_{21}(T_0, T_1, \dots) &= C(T_1, T_2, \dots)\exp(i\omega_{n1}T_0) + D(T_1, T_2, \dots)\exp(i\omega_{n2}T_0) + C.C.
\end{aligned} \tag{3.18}$$

where $C.C.$ represents the complex conjugate. Equations 3.18 are substituted into equations 3.17. It can then be shown that if $\tilde{\omega}_1$ and $\tilde{\omega}_2$ satisfy the following conditions

$$\begin{aligned}
\tilde{\omega}_1 &= \omega_{n1}, \omega_{n2} \\
\tilde{\omega}_2 &= 2\omega_{n1}, 2\omega_{n2}, \omega_{n2} - \omega_{n1}, \omega_{n1} + \omega_{n2},
\end{aligned} \tag{3.19}$$

there will be secular terms on the right-hand side in equation 3.17. For a double pendulum with $\frac{m_2}{m_1} = 20$ and $\frac{l_2}{l_1} = 8$, the ratio of w_{n2} to w_{n1} is approximately 10. So the forcing frequencies for this study are chosen to be w_{n1} in the x direction and $2w_{n1}$ in the y direction.

3.2 Determining the Dimension Required for the Reconstructed Attractor

For a system with known equations of motion, it is easy to determine the dimension of the system. But usually only a few variables can be observed and recorded. It is then necessary to use the time-delay coordinate to reconstruct the attractors. Each point in the reconstructed

attractor has the coordinate $\mathbf{z}_n = (x_{n-m+1}, x_{n-m+2}, \dots, x_{n-1}, x_n)^T$ where x_i is the observable and m is the dimension of the reconstructed attractor. The question now is how many dimensions to use. If too few dimensions are used, points being in a small neighborhood in that specific reconstructed space does not mean that they are actually close to each other. If too many dimensions are used, it will waste a lot of time without improving the result. There are several proposed methods to determine the minimum required dimension. The method of false nearest neighbor will be used in this study. The basis for this method is that in an unfolded attractor (i.e. the attractor reconstructed in high enough dimension), the neighboring points are truly close to each other. There will not be any points that are close to each other due to projection from higher dimensions to lower dimensions. The way to determine if two points in d dimensions are true neighbors is to look at the distance between these two points in $d + 1$ dimensions. The criterion for two points to be false neighbors can thus be written as:

$$\frac{|x_{n+1} - x'_{n+1}|}{R_d(\mathbf{z}_n, \mathbf{z}'_n)} > R_T \quad (3.20)$$

where $R_d(\mathbf{z}_n, \mathbf{z}'_n)$ is the distance between \mathbf{z}_n and \mathbf{z}'_n in d dimension and R_T is the threshold value for false neighbors. For most systems, the threshold value is about 15. There is a possible pitfall in this criterion. If the nearest neighbor of a point is actually very far away from it, then these points will always be considered as true neighbors by the criterion above. It is necessary then to establish a second criterion to check for this possibility.

$$\frac{|x_{n+1} - x'_{n+1}|}{R_A} > 2 \quad (3.21)$$

where R_A is the "nominal radius" of the attractor. The exact definition will not affect the outcome of this criterion. The root mean square (RMS) value of the observable x_n is used in this research. This second criterion will identify a nearest neighbor as false if when going from dimension d to dimension $d + 1$, the added component is of the order of the "nominal diameter" of the attractor. A nearest neighbor is defined as false if it satisfies either one of these criteria.

3.3 Extracting the Unstable Periodic Orbit (UPO) from Data Sets

One of the most important steps in using the OGY control scheme is to identify the unstable periodic orbit. For a system with known equations of motion, it is possible to obtain the UPO by use of a shooting method. Unfortunately, the equations are usually unknown or only partially known in most cases. The only way to obtain the UPO is then to analyze the data set. The most straight forward way to do this is to utilize the concept of a recurrent neighborhood. In short, it is the method of counting the time required for an orbit to return to a pre-defined small neighborhood of the starting point and to choose that time as its period. The problem with this approach is that it usually requires a very large data set and the size of the neighborhood will affect the result of the procedure. So et al. [58] proposed an alternative method to extract a UPO. The basis for the new method is that by applying a transformation to the data set, the transformed data set will cluster around the UPO thus making it possible to identify the UPO by inspecting the histogram of the transformed data. If \mathbf{F} is the mapping function, the transformation used has the following form

$$\hat{\mathbf{z}} = \mathbf{G}(\mathbf{z}, \mathbf{R}) = [\mathbf{I} - \mathbf{S}(\mathbf{z}, \mathbf{R})]^{-1} \cdot [\mathbf{F}(\mathbf{z}) - \mathbf{S}(\mathbf{z}, \mathbf{R}) \cdot \mathbf{z}] \quad (3.22)$$

where \mathbf{I} is the identity matrix and \mathbf{S} is a matrix function of \mathbf{z} and a random tensor \mathbf{R}

$$\mathbf{S}(\mathbf{z}, \mathbf{R}) = \nabla \mathbf{F}(\mathbf{z}) + \mathbf{R} \cdot [\mathbf{F}(\mathbf{z}) - \mathbf{z}]. \quad (3.23)$$

Figure 3.2 illustrates the geometric interpretation of the transformation in one dimension with $\mathbf{R} = 0$. Given a sequence $\{\mathbf{z}_i\}$, $\frac{\mathbf{z}_{n+2} - \mathbf{z}_{n+1}}{\mathbf{z}_{n+1} - \mathbf{z}_n}$ is the slope of the line γ . It is also an estimate of the Jacobian at \mathbf{z}_n . From the geometry in figure 3.2, we obtain the following equation

$$\frac{\hat{\mathbf{z}}_n - \mathbf{z}_{n+1}}{\hat{\mathbf{z}}_n - \mathbf{z}_n} = \frac{\mathbf{z}_{n+2} - \mathbf{z}_{n+1}}{\mathbf{z}_{n+1} - \mathbf{z}_n} \approx \nabla \mathbf{F}(\mathbf{z}_n). \quad (3.24)$$

When equation 3.24 is solved for $\hat{\mathbf{z}}_n$, the result is

$$\hat{\mathbf{z}}_n \approx \frac{\mathbf{z}_{n+1} - \mathbf{z}_n \nabla \mathbf{F}(\mathbf{z}_n)}{1 - \nabla \mathbf{F}(\mathbf{z}_{n+1})} = \frac{\mathbf{F}(\mathbf{z}_n) - \mathbf{z}_n \nabla \mathbf{F}(\mathbf{z}_n)}{1 - \nabla \mathbf{F}(\mathbf{z}_{n+1})}. \quad (3.25)$$

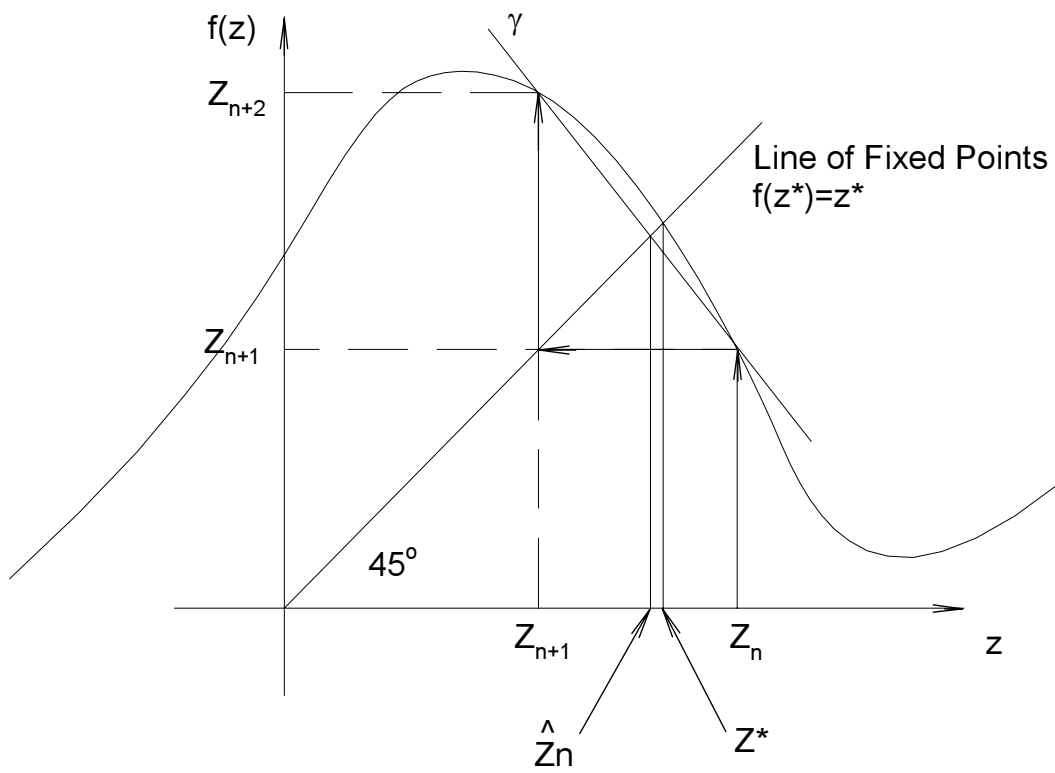


Figure 3.2: Geometric Interpretation of the Transformation in One Dimension for the Case $\mathbf{R} = 0$

Comparing equation 3.25 with equations 3.22 and 3.23. It is clear that the point $\hat{\mathbf{z}}_n$ is the image of \mathbf{z}_n under the map $\mathbf{G}(\mathbf{z}, 0)$, that is,

$$\hat{\mathbf{z}}_n = \mathbf{G}(\mathbf{z}_n, 0). \quad (3.26)$$

In the special case $\mathbf{R} = 0$, not only do the fixed points have peaks in the histogram of the transformed data set, but the point $\mathbf{G}(\bar{\mathbf{z}})$ may also have a peak in the histogram of the transformed data set if $\nabla \mathbf{G}(\bar{\mathbf{z}}) = \mathbf{0}$. The addition of a number of random \mathbf{R} s has the effect of scattering the points that are not fixed points such that they will not have a peak in the histogram.

The transformation 3.22 has the following properties:

- If \mathbf{z}^* is a fixed point of the mapping function \mathbf{F} , then \mathbf{z}^* is also a fixed point of the transformation $\mathbf{G}(\mathbf{z}, \mathbf{R})$. (i.e. $\mathbf{G}(\mathbf{z}^*, \mathbf{R}) = \mathbf{z}^*$)
- If \mathbf{z}^* is a fixed point of the mapping function \mathbf{F} , then \mathbf{z}^* is a stationary point of the transformation $\mathbf{G}(\mathbf{z}, \mathbf{R})$. (i.e. $\nabla \mathbf{G}(\mathbf{z}^*, \mathbf{R}) = 0$)
- The pointwise dimension of the attractor at \mathbf{z} is unchanged if \mathbf{z} is a regular point. The dimension will typically be halved under the transformation \mathbf{G} if \mathbf{z} is a stationary point of \mathbf{G} .

The proof for the first property is straightforward. The paper by So et al. [58] has a detailed proof for the second and third properties. In appendix B, the extractions of the UPO from the logistic map and the Hénon map using the transformation are presented as examples of this approach.

3.4 Control

One of the first attempts to control a chaotic system was the Ott-Grebog-Yorke (OGY) method [40]. The basic principle for this method is that there are infinitely many unstable

periodic orbits (UPOs) embedded in the strange attractor and eventually the orbit will be in close neighborhoods of all of them. Once the orbit travels to the neighborhood of the target UPO, it is then possible to adjust an available system parameter based on a linear approximation in the neighborhood such that the next iteration will put the orbit on the stable manifold of the target UPO. In figure 3.3 the original OGY control procedure is illustrated. Assume that p is a system parameter that can be varied around a nominal value p_0 . Let $\boldsymbol{\xi}_F(p_0)$ be the desired unstable periodic point and λ_s and λ_u be the corresponding stable and unstable eigenvalues when $p = p_0$. Let \mathbf{e}_s and \mathbf{e}_u be the unit vectors in the stable and unstable directions. The contravariant basis vectors \mathbf{f}_s and \mathbf{f}_u are defined by

$$\mathbf{f}_s \cdot \mathbf{e}_s = \mathbf{f}_u \cdot \mathbf{e}_u = 1 \quad (3.27)$$

$$\mathbf{f}_s \cdot \mathbf{e}_u = \mathbf{f}_u \cdot \mathbf{e}_s = 0. \quad (3.28)$$

Assume that the periodic point shifts to $\boldsymbol{\xi}_F(p_0 + \bar{p})$ when $p = p_0 + \bar{p}$. For small \bar{p} , $\boldsymbol{\xi}_F(p_0 + \bar{p})$ can be approximated as

$$\boldsymbol{\xi}_F(p_0 + \bar{p}) \approx \boldsymbol{\xi}_F(p_0) + \bar{p}\mathbf{g} \quad (3.29)$$

where $\mathbf{g} = \left. \frac{\partial \boldsymbol{\xi}_F(p)}{\partial p} \right|_{p=p_0}$. In the neighborhood of $\boldsymbol{\xi}_F(p_0)$, the mapping can be approximated as

$$\boldsymbol{\xi}_{n+1} - \boldsymbol{\xi}_F(p_0 + p_n) = \mathbf{M} \cdot [\boldsymbol{\xi}_n - \boldsymbol{\xi}_F(p_0 + p_n)] \quad (3.30)$$

where \mathbf{M} can be approximated as

$$\mathbf{M} = \lambda_u \mathbf{e}_u \mathbf{f}_u + \lambda_s \mathbf{e}_s \mathbf{f}_s. \quad (3.31)$$

Substituting equation 3.29 and equation 3.31 into equation 3.30, the equation becomes

$$\boldsymbol{\xi}_{n+1} - \boldsymbol{\xi}_F(p_0) \approx p_n \mathbf{g} + (\lambda_u \mathbf{e}_u \mathbf{f}_u + \lambda_s \mathbf{e}_s \mathbf{f}_s) \cdot [\boldsymbol{\xi}_n - \boldsymbol{\xi}_F(p_0) - p_n \mathbf{g}]. \quad (3.32)$$

The purpose of the OGY control is to choose p_n such that $\mathbf{f}_u \cdot (\boldsymbol{\xi}_{n+1} - \boldsymbol{\xi}_F(p_0)) = 0$. Dot equation 3.32 with \mathbf{f}_u and solve for p_n

$$p_n = \frac{\lambda_u}{\lambda_u - 1} \frac{\mathbf{f}_u \cdot [\boldsymbol{\xi}_n - \boldsymbol{\xi}_F(p_0)]}{\mathbf{f}_u \cdot \mathbf{g}}. \quad (3.33)$$

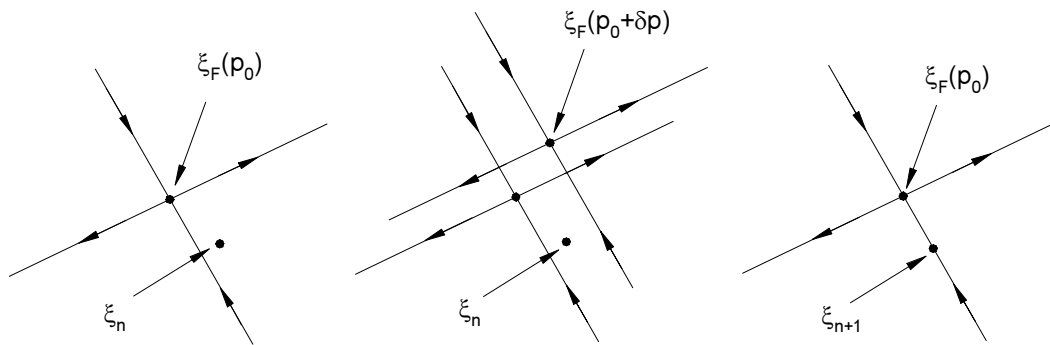


Figure 3.3: Illustration of the OGY Control Procedure (from Ditto et al., 1990 [12])

As indicated by Dressler and Nitsche ([14], [38]), it is possible to lose control if the time delay coordinates are used instead of the real state variables. The original OGY also failed to address the problem of higher dimensional systems with more than one unstable direction. Ding et al. [11] proposed an extension to the original OGY to accommodate these two concerns. Assume that the system has a dimension m when using the time delay coordinates. The coordinate of the n -th point is

$$\mathbf{z}_n = \begin{pmatrix} z_n^{(1)} \\ z_n^{(2)} \\ \vdots \\ z_n^{(m)} \end{pmatrix} = \begin{pmatrix} x_{n-m+1} \\ x_{n-m+2} \\ \vdots \\ x_n \end{pmatrix}. \quad (3.34)$$

The map for \mathbf{z}_n will then be

$$\mathbf{z}_{n+1} = \mathbf{G}(\mathbf{z}_n, p_{n-m+1}, p_{n-m+2}, \dots, p_n) \quad (3.35)$$

where p_i is the parameter at iteration i . The Jacobian of the map at \mathbf{z} is

$$\mathbf{A} = \mathbf{D}_{\mathbf{z}}\mathbf{G}(\mathbf{z}_n, p_{n-m+1}, p_{n-m+2}, \dots, p_n). \quad (3.36)$$

Define a set of m -dimensional column vectors

$$\begin{aligned} \mathbf{B}^{(m)} &= D_{p_{n-m+1}}\mathbf{G}(\mathbf{z}_n, p_{n-m+1}, p_{n-m+2}, \dots, p_n) \\ \mathbf{B}^{(m-1)} &= D_{p_{n-m+2}}\mathbf{G}(\mathbf{z}_n, p_{n-m+1}, p_{n-m+2}, \dots, p_n) \\ &\vdots \\ \mathbf{B}^{(1)} &= D_{p_n}\mathbf{G}(\mathbf{z}_n, p_{n-m+1}, p_{n-m+2}, \dots, p_n). \end{aligned} \quad (3.37)$$

Assume that $\bar{\mathbf{z}}$ is a fixed point of the system when $p = \bar{p}$

$$\bar{\mathbf{z}}(\bar{p}) = \mathbf{G}(\bar{\mathbf{z}}(\bar{p}), \bar{p}, \bar{p}, \dots, \bar{p}). \quad (3.38)$$

The mapping near the fixed point can then be written as

$$\mathbf{z}_{n+1} - \bar{\mathbf{z}}(\bar{p}) = \mathbf{A}(\mathbf{z}_n - \bar{\mathbf{z}}(\bar{p})) + \mathbf{B}^{(m)}(p_{n-m+1} - \bar{p}) + \mathbf{B}^{(m-1)}(p_{n-m+2} - \bar{p}) + \dots + \mathbf{B}^{(1)}(p_n - \bar{p}) \quad (3.39)$$

where \mathbf{A} and $\mathbf{B}^{(i)}$ are evaluated at $\bar{\mathbf{z}}(\bar{p})$ and $p_{n-m+1} = p_{n-m+2} = \dots = p_n = \bar{p}$. Due to the nature of the discrete-time series and delay coordinates used here, \mathbf{A} and \mathbf{B} 's have the following form.

$$\mathbf{A} = \begin{pmatrix} 0 & 1 & 0 & \dots & 0 \\ 0 & 0 & 1 & \dots & 0 \\ \vdots & \vdots & \vdots & \vdots & \vdots \\ 0 & 0 & 0 & \dots & 1 \\ a^{(m)} & a^{(m-1)} & a^{(m-2)} & \dots & a^{(1)} \end{pmatrix}_{m \times m} \quad (3.40)$$

$$\mathbf{B}^{(i)} = \begin{pmatrix} 0 \\ 0 \\ \vdots \\ 0 \\ b^{(i)} \end{pmatrix}_{m \times 1} \quad (3.41)$$

Now, introduce the state-plus-parameters system which includes \mathbf{z}_n and the previous parameter

$$\mathbf{Y}_n = \begin{pmatrix} \mathbf{z}_n \\ p_{n-m+1} \\ p_{n-m+2} \\ \vdots \\ p_n \end{pmatrix}_{(2m-1) \times 1} \quad (3.42)$$

The fixed point for this expanded phase space is then

$$\bar{\mathbf{Y}} = \begin{pmatrix} \bar{\mathbf{z}}(\bar{p}) \\ \bar{p} \\ \bar{p} \\ \vdots \\ \bar{p} \end{pmatrix}_{(2m-1) \times 1} \quad (3.43)$$

Now equation 3.39 can be rewritten as

$$\mathbf{Y}_{n+1} - \bar{\mathbf{Y}} = \tilde{\mathbf{A}}(\mathbf{Y}_n - \bar{\mathbf{Y}}) + \tilde{\mathbf{B}}(p_n - \bar{p}) \quad (3.44)$$

where

$$\tilde{\mathbf{A}} = \begin{pmatrix} \mathbf{A} & \mathbf{B}^{(m)} & \mathbf{B}^{(m-1)} & \mathbf{B}^{(m-2)} & \dots & \mathbf{B}^{(2)} \\ \mathbf{0} & 0 & 1 & 0 & \dots & 0 \\ \mathbf{0} & 0 & 0 & 1 & \dots & 0 \\ \vdots & \vdots & \vdots & \vdots & \vdots & \vdots \\ \mathbf{0} & 0 & 0 & 0 & \dots & 1 \\ \mathbf{0} & 0 & 0 & 0 & \dots & 0 \end{pmatrix}_{(2m-1) \times (2m-1)} \quad (3.45)$$

and

$$\tilde{\mathbf{B}} = \begin{pmatrix} \mathbf{B}^{(1)} \\ 0 \\ \vdots \\ 0 \\ 1 \end{pmatrix}_{(2m-1) \times 1} \quad (3.46)$$

Assume that \mathbf{A} has u unstable directions and s stable directions ($u + s = m$) with eigenvalues $|\lambda_1| > |\lambda_2| > \dots > |\lambda_u| > 1 > |\lambda_{u+1}| > |\lambda_{u+2}| > \dots > |\lambda_m|$. Let \mathbf{e}_i be the corresponding eigenvectors. Then $\lambda_1, \lambda_2, \dots, \lambda_m$ are also the eigenvalues of $\tilde{\mathbf{A}}$ with corresponding eigenvectors

$$\mathbf{k}_i = \begin{pmatrix} \mathbf{e}_i \\ 0 \\ \vdots \\ 0 \\ 0 \end{pmatrix}_{(2m-1) \times 1} \quad (3.47)$$

$i = 1, 2, \dots, m$. As indicated by Ding et al. [11], the $(m - 1)$ vectors that span the null space of $\tilde{\mathbf{A}}^{m-1}$ along with $\mathbf{k}_{u+1}, \mathbf{k}_{u+2}, \dots, \mathbf{k}_m$ form the basis of the stable subspace of $\tilde{\mathbf{A}}$.

The goal of the control is to make u parametric perturbations $\delta p_n, \delta p_{n+1}, \dots, \delta p_{n+u-1}$ such that $\delta \mathbf{Y}_{n+u} = \mathbf{Y}_{n+u} - \bar{\mathbf{Y}}$ is entirely in the stable subspace of $\tilde{\mathbf{A}}$. The contravariant unstable eigenvectors \mathbf{v}_i ($i = 1, 2, \dots, u$) can be obtained by solving

$$\tilde{\mathbf{A}}^T \mathbf{v}_i = \lambda_i \mathbf{v}_i \quad (3.48)$$

where $\tilde{\mathbf{A}}^T$ is the transpose of $\tilde{\mathbf{A}}$. These contravariant unstable eigenvectors are perpendicular to the stable subspace of $\tilde{\mathbf{A}}$. By choosing $\delta p_n, \delta p_{n+1}, \dots, \delta p_{n+u-1}$ such that

$$\begin{aligned} \mathbf{v}_1^T \delta \mathbf{Y}_{n+u} &= 0 \\ \mathbf{v}_2^T \delta \mathbf{Y}_{n+u} &= 0 \\ &\vdots \\ \mathbf{v}_u^T \delta \mathbf{Y}_{n+u} &= 0, \end{aligned} \quad (3.49)$$

$\delta \mathbf{Y}_{n+u}$ is in the stable subspace of $\tilde{\mathbf{A}}$. By combining equation 3.44 and equation 3.49, the control law for the control parameter p_n at time n can be found to be

$$p_n = \bar{p} - \left(\frac{\lambda_1}{(\mathbf{v}_1^T \tilde{\mathbf{B}})} \mathbf{v}_1^T \right) \delta \mathbf{Y}_n \quad (3.50)$$

for $u = 1$ and

$$p_n = \bar{p} - \left(\sum_{k=1}^u \frac{(\lambda_k)^u}{(\mathbf{v}_k^T \tilde{\mathbf{B}}) \prod_{i=1, i \neq k}^u (\lambda_k - \lambda_i)} \mathbf{v}_k^T \right) \delta \mathbf{Y}_n \quad (3.51)$$

for $u > 1$. Although it is possible to calculate $p_{n+1}, p_{n+2}, \dots, p_{n+u-1}$, it is preferable to calculate p_n at every iterate n because of the possible presence of system noise.

Chapter 4

Numerical Result

4.1 Chaos

The system used in this research has the following parameter values: $l_1 = 4m$, $l_2 = 24m$, $m_1 = 250kg$, and $m_2 = 5000kg$. The non-dimensional parameters used in equations 3.11, 3.12 are $m = \frac{5000}{250+5000}$ and $l = \frac{4}{24}$. The non-dimensional friction coefficients are $\mu_1 = \mu_2 = 0.1$.

When the base point oscillations in the horizontal and vertical directions are small, the system will be oscillating periodically. As the magnitude of the motions of the base point grows, the system eventually goes into chaos. Figure 4.1 to figure 4.4 are the projections of the attractor onto various planes for $\delta = 0.25$ and $\eta = 0.45$ ¹.

In figure 4.5, we see the FFT of θ_1 , θ_2 , $\dot{\theta}_1$, and $\dot{\theta}_2$. These figures show that the system is possibly chaotic. From this point on, the numerical integration will be treated as a black box for producing data and only $\dot{\theta}_2$ will be used as an observable for further study. The first thing to do with the observed time series is to plot the n -th value against the $(n+1)$ -th value to see if there is some structure. Figure 4.6 is such a plot for the observable $\dot{\theta}_2$ and it seems

¹As defined in equations 3.10, δ is the ratio of the amplitude of base point oscillation in the horizontal direction to the length of the lower part of the double pendulum. η is the ratio in the vertical direction.

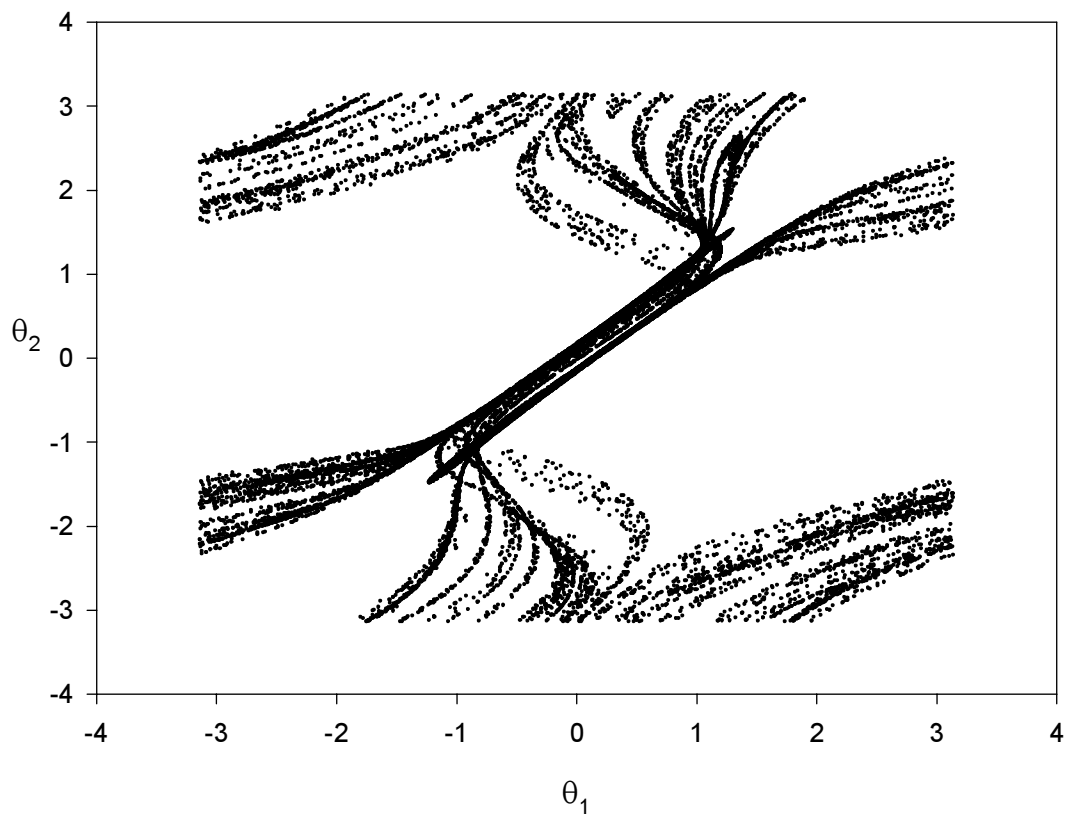


Figure 4.1: θ_1 vs θ_2

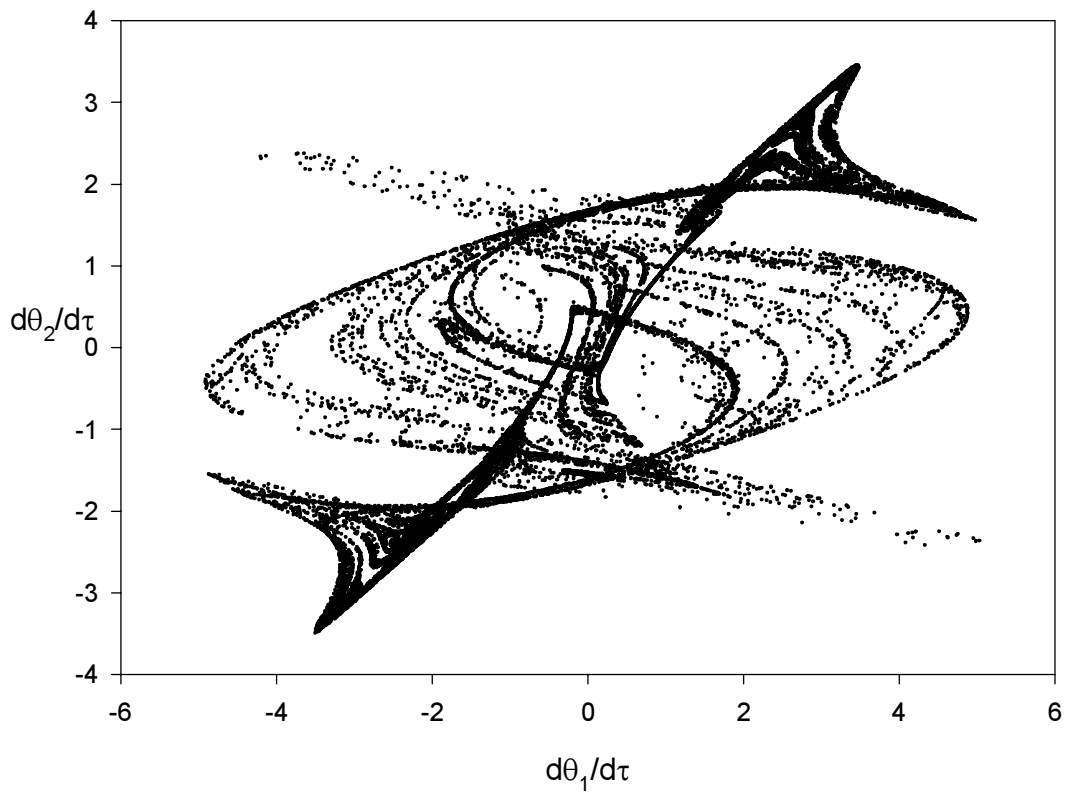


Figure 4.2: $\dot{\theta}_1$ vs $\dot{\theta}_2$

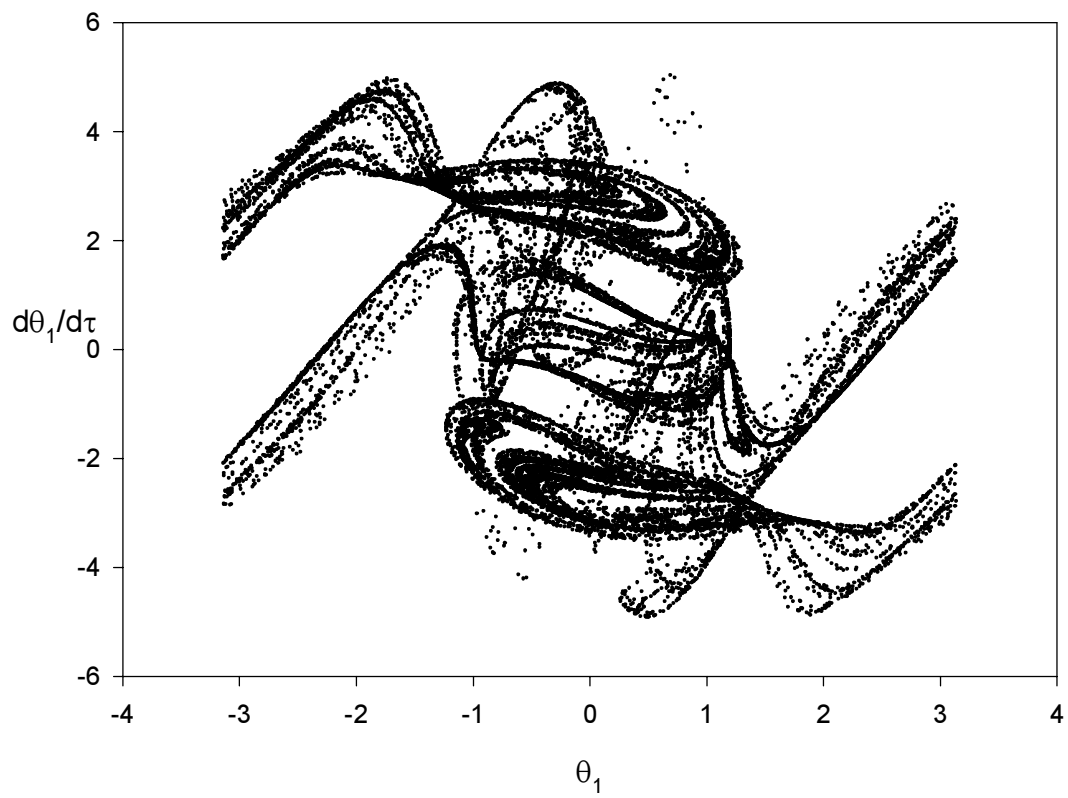


Figure 4.3: θ_1 vs $\dot{\theta}_1$

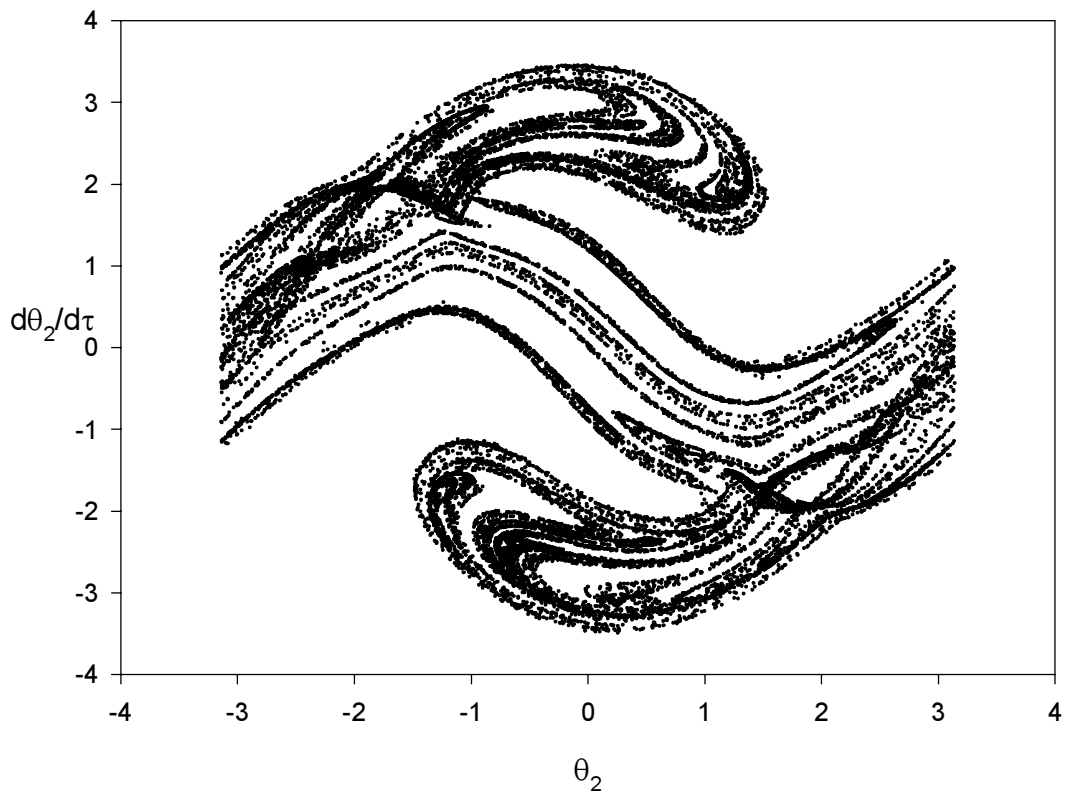


Figure 4.4: θ_2 vs $\dot{\theta}_2$

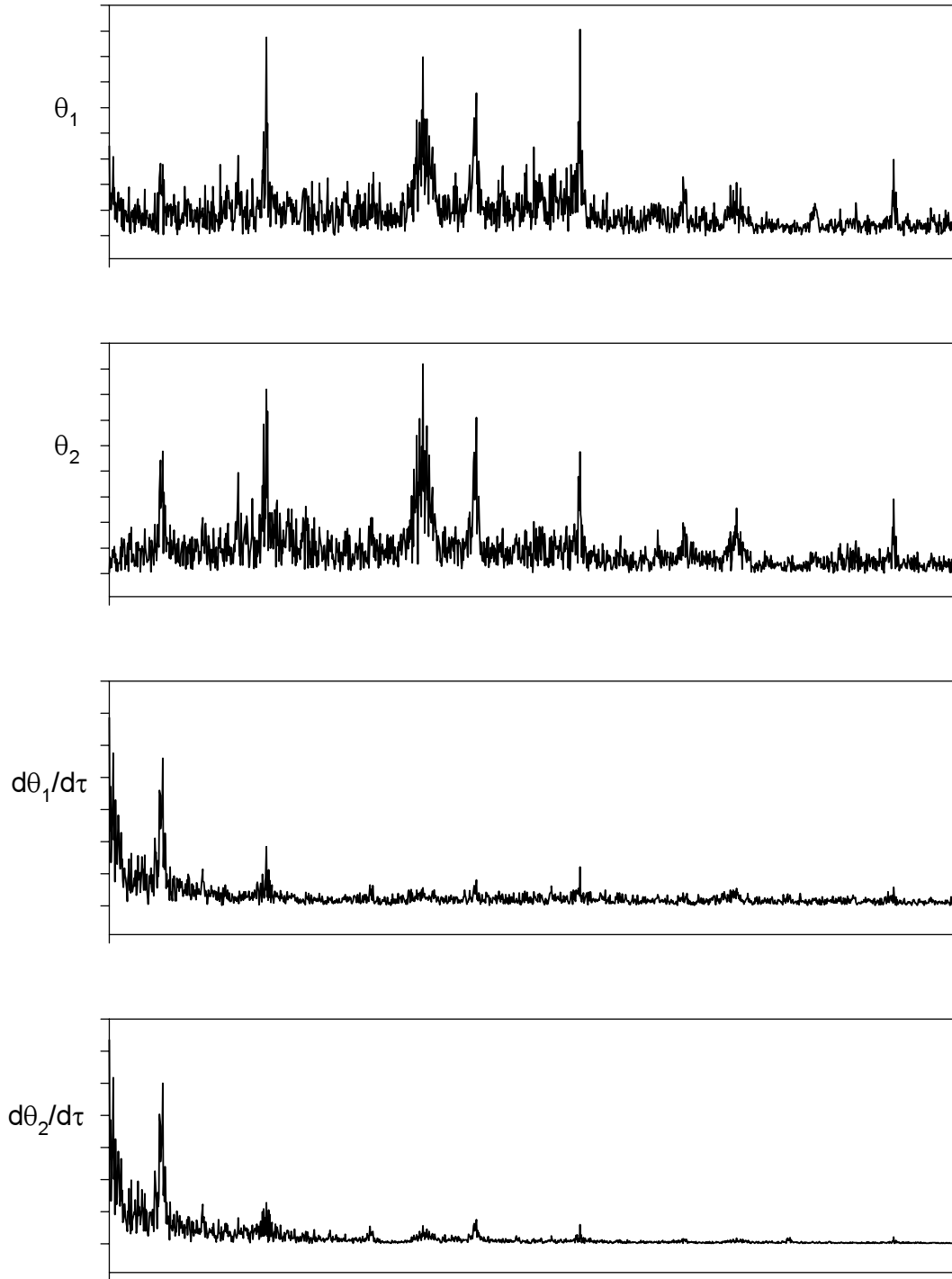


Figure 4.5: FFTs of θ_1 , θ_2 , $\dot{\theta}_1$, and $\dot{\theta}_2$

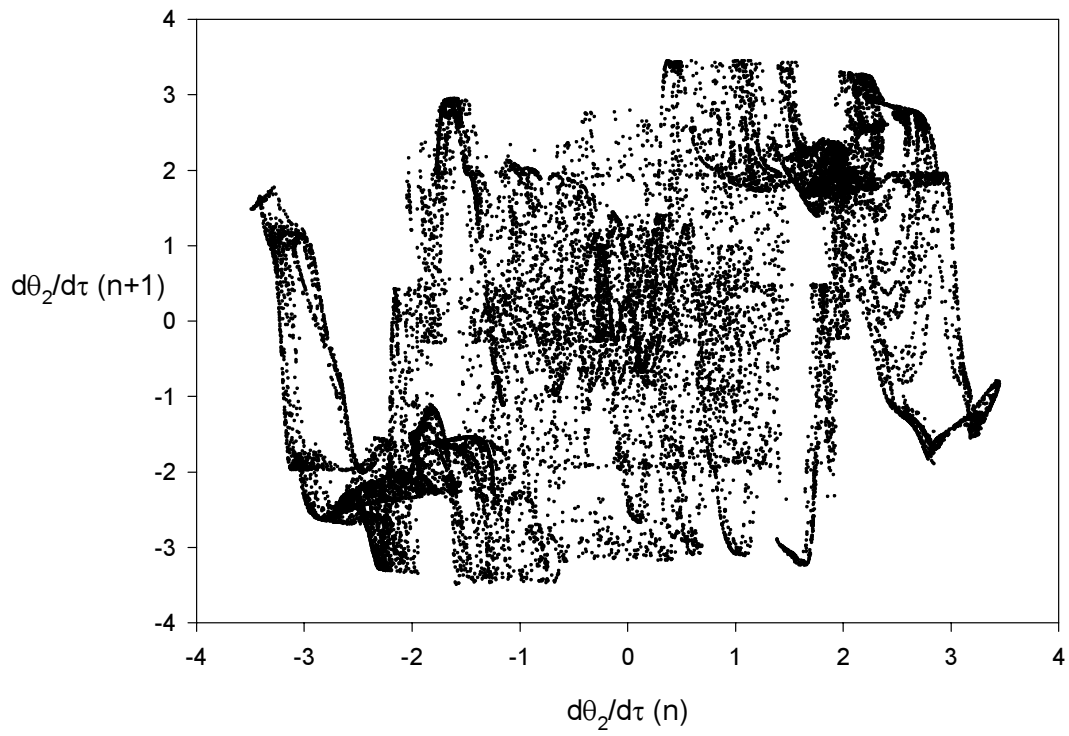


Figure 4.6: $\dot{\theta}_2(n)$ vs $\dot{\theta}_2(n + 1)$

to be some strange-attractor-like structure. To determine if the system is chaotic, it is then necessary to determine the largest Lyapunov exponent. The algorithm developed by Kantz [25] is used here. The basic idea of the Kantz algorithm is the following. Choose N points in the data set $\{\beta_1, \beta_2, \dots, \beta_N\}$. For each point β_n , select all its neighbors whose distances from β_n are less than ϵ . Let $\mathbf{d}(\beta_n, \epsilon, \Delta n)$ be the average distance of all the neighbors of β_n as a function of the iteration Δn . Define the function $\mathbf{S}(\Delta n)$ as

$$\mathbf{S}(\Delta n) = \frac{1}{N} \sum_{n=1}^N \ln(\mathbf{d}(\beta_n, \epsilon, \Delta n)). \quad (4.1)$$

In the region where $\mathbf{S}(\Delta n)$ exhibits linear increase, the slope of $\mathbf{S}(\Delta n)$ is then an estimate of the maximum Lyapunov exponent. Figure 4.7 is the result obtained from the program in the TISEAN package (see R. Hegger, H. Kantz, and T. Schreiber [21]). The slope of the dashed line is the maximum Lyapunov exponent. In this case, the maximum Lyapunov exponent is approximately 1.069 which indicates that the system is chaotic.

4.2 Dimension of Embedding

When only one motion observable is available, it is necessary to use the time-delay coordinate method to reconstruct the attractor. It is important to determine the embedding dimension required to appropriately reconstruct the attractor. For this study, the method of the false nearest neighbor is used to accomplish this goal. Figure 4.8 is the result of applying the false-nearest-neighbor analysis to a data set of 50000 points. From the figure, the percentage of false nearest neighbors decreases rapidly from an embedded dimension 1 to an embedded dimension 3. After dimension 3, the rate of decrease levels off and after dimension 5, the decrease is almost negligible. Instead of going to zero, the percentage remains about 10 percent after dimension 5. There are two possible explanations. The first one is the presence of noise in the data set. For this study, the data were generated from a numerical experiment. Noise should not be a factor here. The second possible explanation lies in the false nearest neighbor method itself. Geometry is the only consideration here. It is possible that in some

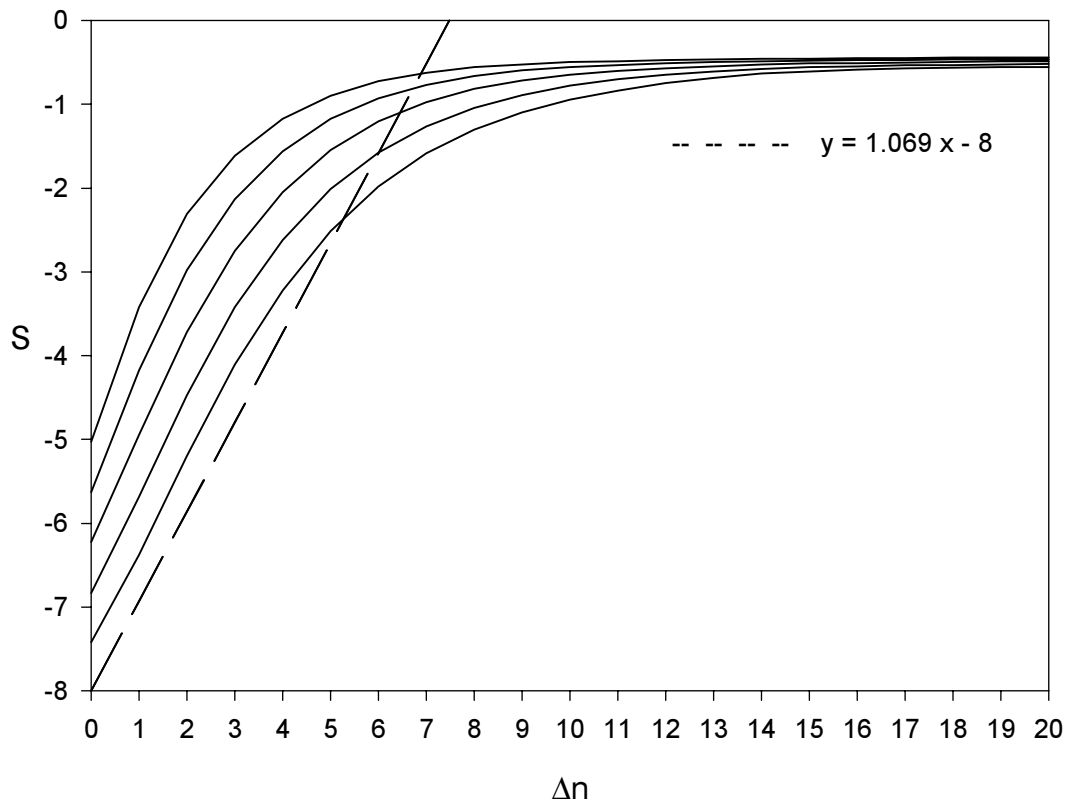


Figure 4.7: Estimation of the Maximum Lyapunov Exponent

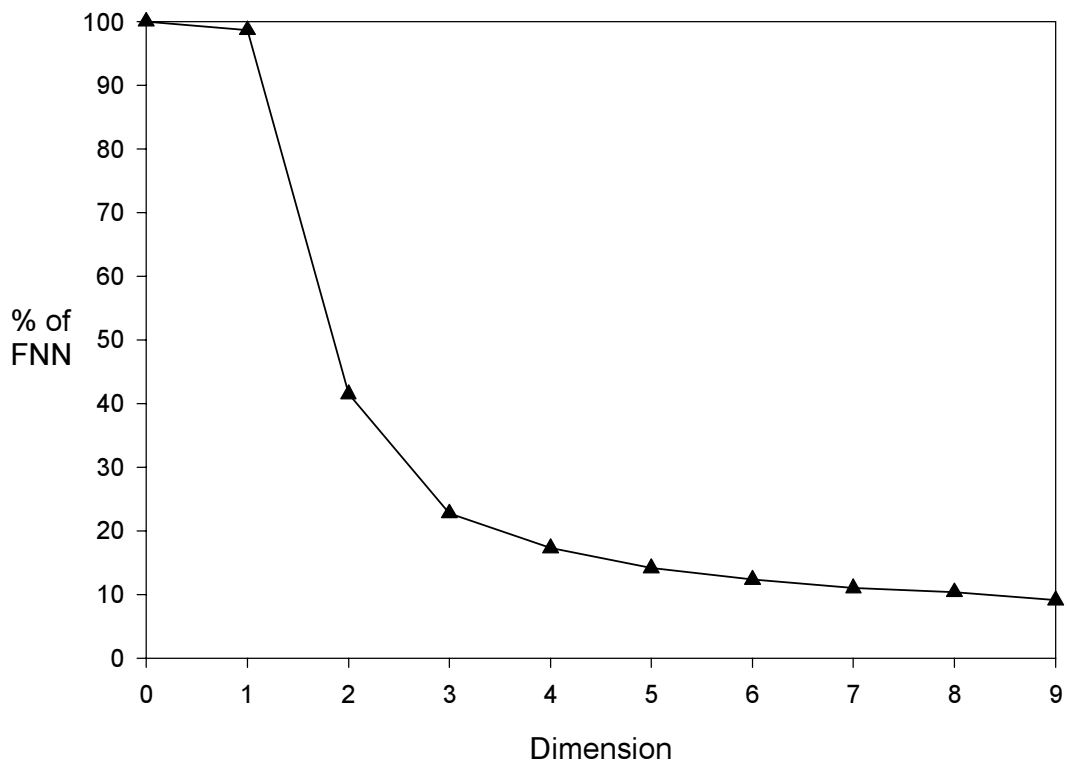


Figure 4.8: The Result of the False Nearest Neighbor Analysis

region on the attractor, the unstable eigenvalues are large enough such that even a true nearest neighbor will not be able to satisfy the criteria. There are two points to consider when trying to determine the required embedded dimension

- The decrease of the percentage of false nearest neighbors from dimension 3 to dimension 9 is about 10 percent while the decrease is about 20 percent from dimension 2 to dimension 3.
- The false-nearest-neighbor analysis gives an indication of the global dimension of the attractor. The OGY control scheme needs the local behavior near an unstable fixed point. The local dimension near an unstable fixed point is not necessarily smaller than the global dimension but it usually is.

With these considerations, an embedded dimension of 3 seems to be a good starting point.

4.3 Determining the Fixed Point

Once the embedded dimension is chosen, the next step is to determine the location of a fixed point. The transform method is used here instead of the close return method. The same data set is used again. 500 different random \mathbf{R} s are used in the transforms. It is hard to visualize a general histogram of points in 3 dimensions. Since time-delay coordinates are used in this study, the fixed point will be on the diagonal line $x_1 = x_2 = x_3$. Instead of trying to visualize the general histogram, it is possible to determine the peak by looking at the one-dimension histogram of x_1 , x_2 , and x_3 components of all points in the transformed data set that are near the diagonal. Figure 4.9 is the result. The histogram on top is obtained by applying the fixed point transformation on the first 2000 points in the data set. The plot at the bottom is the result by applying the method to the whole data set (50000 points). From the histograms, it is determined that the point $(-2.498, -2.498, -2.498)$ is a fixed point. The UPO Analyzer routine in Nonlinear Dynamics Toolbox package (NDT, a software package

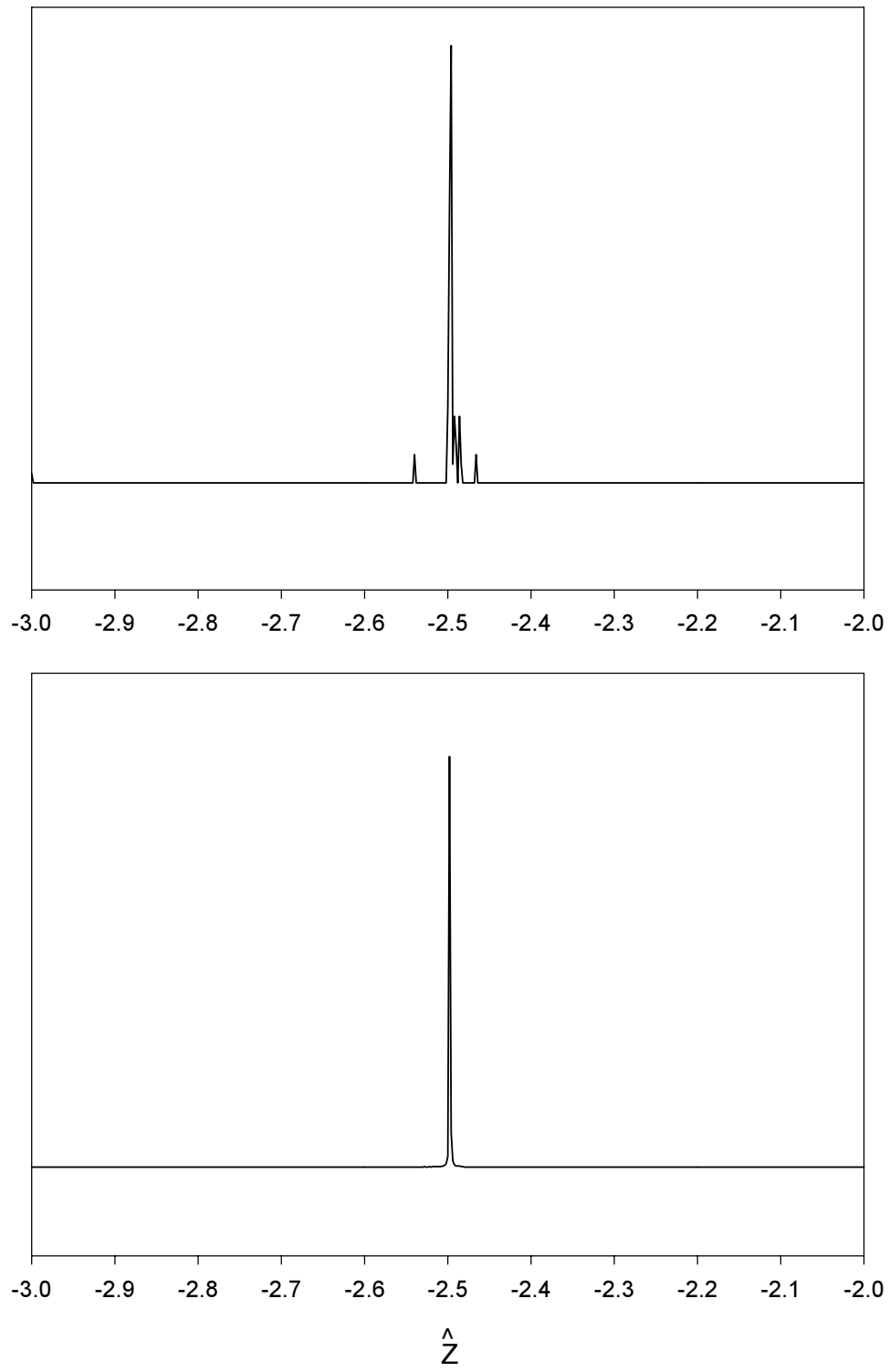


Figure 4.9: Histogram of the Transformed Data Set

developed by a research group at Georgia Tech) uses the close return method to locate UPO. It also identifies this point as a fixed point when the whole data set is used. It is not able to do that from the first 2000 points of the data set. This shows that the fixed point transform method can identify the fixed point using a shorter data set.

4.4 Control Using Horizontal Oscillation of the Base Point as the Control Parameter

In order to use the control scheme, it is necessary to obtain the Jacobian at the fixed point and the sensitivity vector (the differential of the mapping function with respect to the control parameter). The Jacobian is obtained by collecting points in a predefined neighborhood of the fixed point (x^*, x^*, x^*) . The method of least squares is then used to find the Jacobian. For dimension $d = 3$, the Jacobian has the form:

$$\nabla \mathbf{F} = \begin{pmatrix} 0 & 1 & 0 \\ 0 & 0 & 1 \\ a^{(3)} & a^{(2)} & a^{(1)} \end{pmatrix}. \quad (4.2)$$

After determining the Jacobian, the sensitivity can be obtained in the following manner: If the orbit at iteration n , x_n , is in a predefined neighborhood of the fixed point, change the control parameter to $p = p_0 + \delta p_n$ where p_0 is the nominal value of the control parameter. Iterate once and collect the value x_{n+1} . Change the parameter back to p_0 and iterate twice more to collect x_{n+2} and x_{n+3} . The sensitivity vector $(b^{(1)}, b^{(2)}, b^{(3)})$ can then be approximately calculated as

$$\begin{aligned} b^{(1)} &= \frac{\delta x_{n+1} - a^{(1)}\delta x_n - a^{(2)}\delta x_{n-1} - a^{(3)}\delta x_{n-2}}{\delta p_n} \\ b^{(2)} &= \frac{\delta x_{n+2} - a^{(1)}\delta x_{n+1} - a^{(2)}\delta x_n - a^{(3)}\delta x_{n-1}}{\delta p_n} \\ b^{(3)} &= \frac{\delta x_{n+3} - a^{(1)}\delta x_{n+2} - a^{(2)}\delta x_{n+1} - a^{(3)}\delta x_n}{\delta p_n} \end{aligned} \quad (4.3)$$

where $\delta x_i = x_i - x^*$. After acquiring the Jacobian and the sensitivity vector, it is then possible to apply the control on the system.

For all cases in this section, the maximum allowable change of the control parameter is 5.0×10^{-2} . Figure 4.10 shows the result of applying control on the system. The only restriction on the control parameter is that it has to be less than the maximum allowable change. For this study, the allowable maximum change of the parameter is 0.05. If the calculated change is larger than the maximum, then no change is applied. The figure at the bottom shows the portion of the figure at the top around the fixed point. Figure 4.11 shows the control parameter at each iteration. With the exception of the initial period of the control, the parameter change used is very small ($\approx 2.0 \times 10^{-4}$).

In real physical systems, there are two things that need to be taken into consideration. First, the system can not apply parameter changes below a certain minimum. Second, the system may not be able to apply arbitrary parameter change between the maximum allowable change and the minimum change. Figure 4.12 shows the result of applying control with both the minimum and maximum restriction. The minimum is 1.0×10^{-2} for this case. The plot on the top is similar to the one in figure 4.10. But the plot at the bottom shows that there is a small variation around the fixed point due to the restriction of a minimum change of control parameter. Figure 4.13 shows the control parameter at each iteration under the restriction. Figure 4.14 shows the control with the restriction that the parameter change can only occur at certain values that are less than the maximum. Figure 4.15 shows the control parameter at each iteration under such a restriction. The step size for this case is 1.0×10^{-2} .

To quantify the effect of the minimum value and discrete value restrictions, the average value and standard deviation of the observable motion under control are calculated for several different minimums and step sizes. Table 4.1 gives the average and standard deviation of the observable motion that is under control. Figure 4.16 is the plot of the values in table 4.1. The average value does not change much for different minimum or step size. The standard deviation, on the other hand, increases as the minimum or step size increases. There

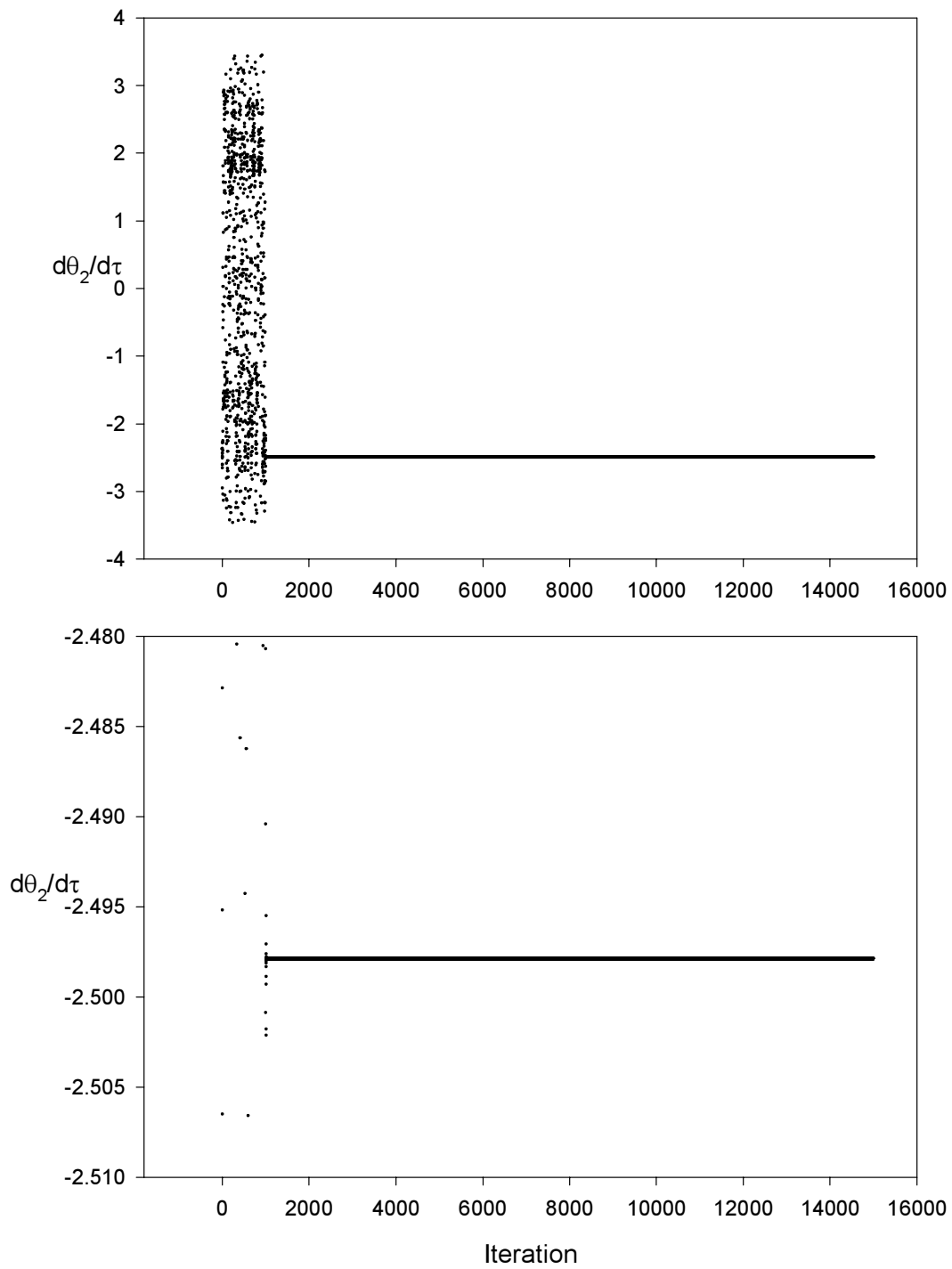


Figure 4.10: Control of the System with Only Maximum Restriction on the Control Parameter

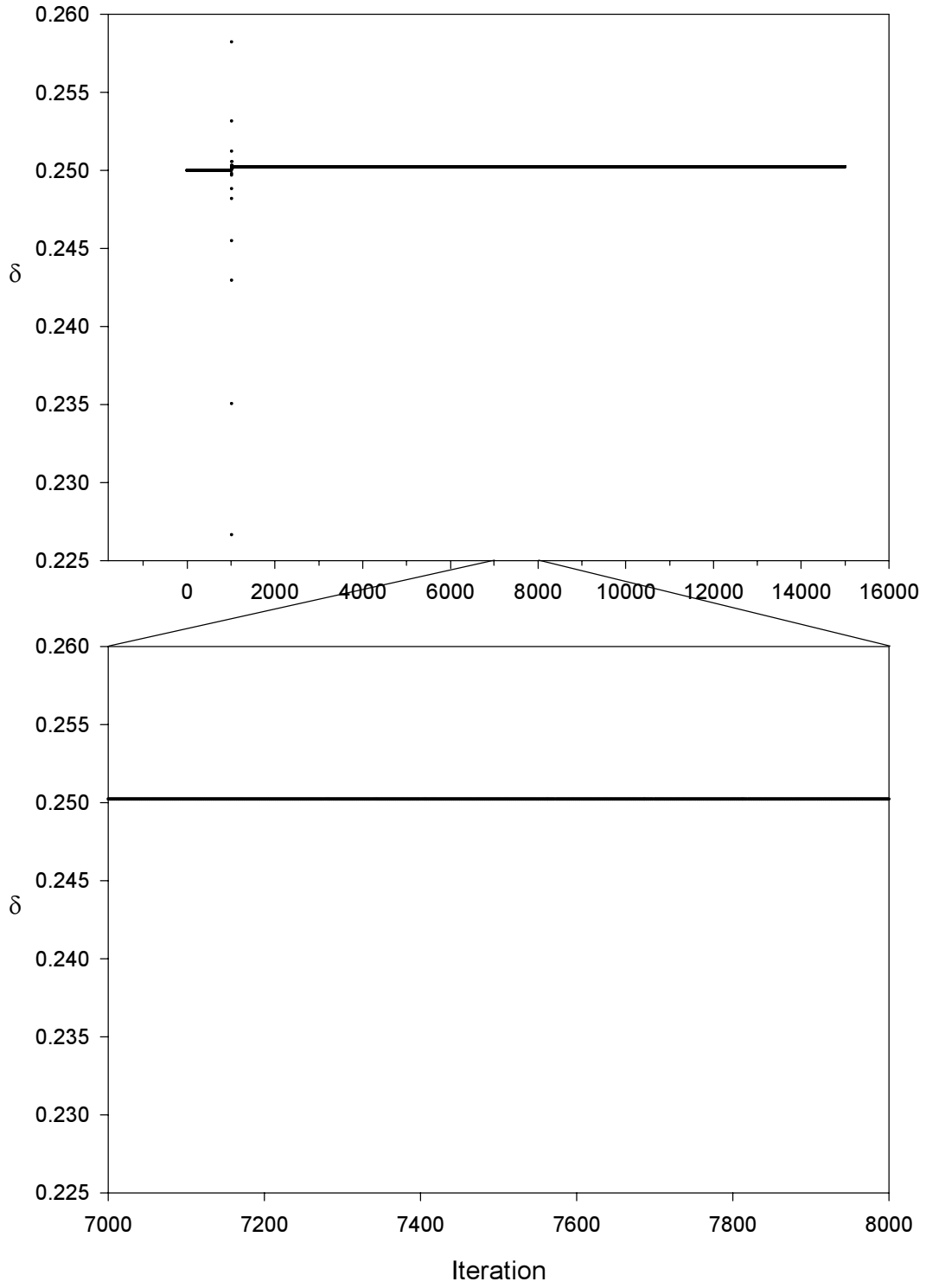


Figure 4.11: Scatter Plot of the Control Parameter at Each Iteration

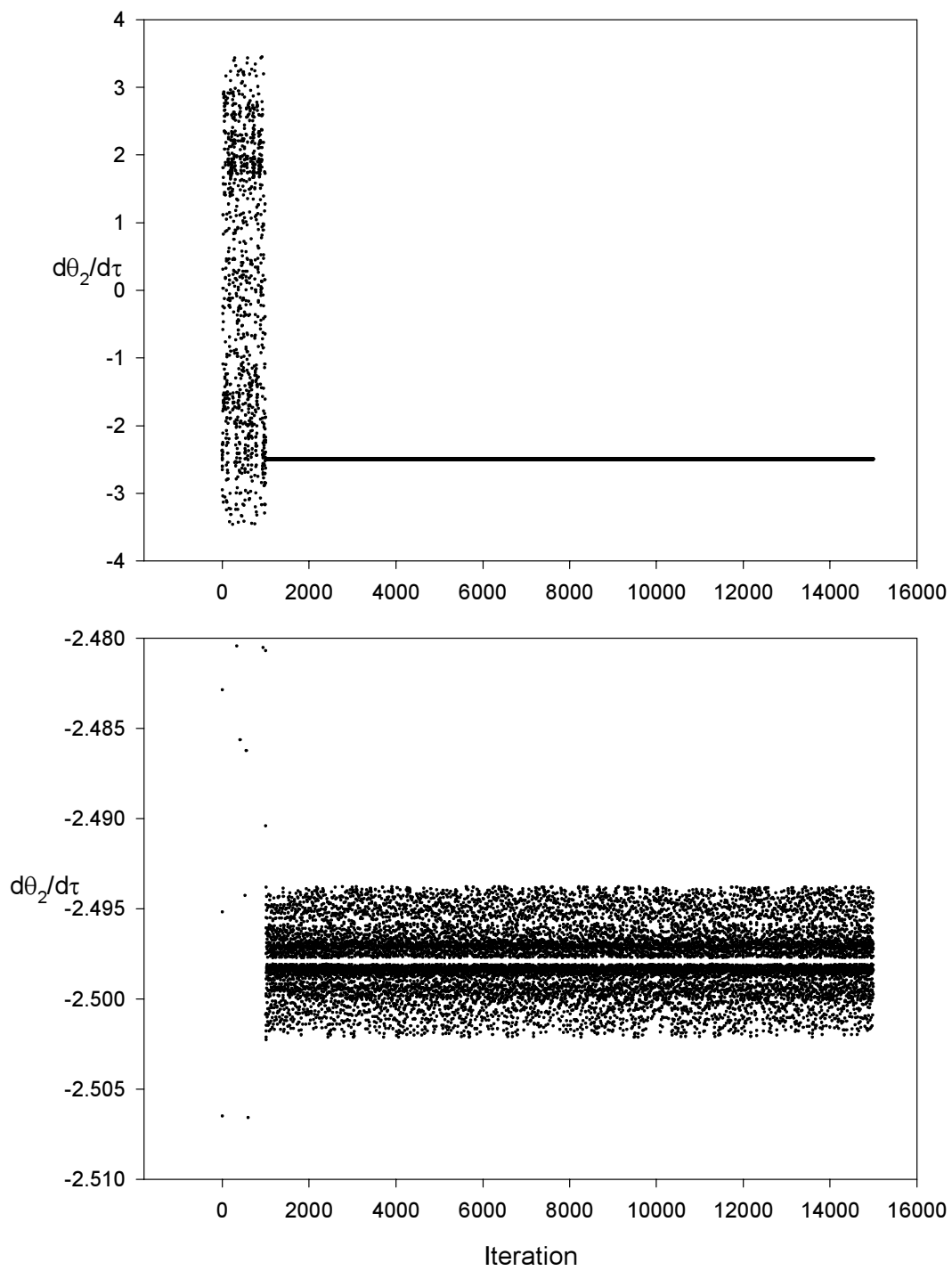


Figure 4.12: Control with Both Minimum and Maximum Restriction on the Control Parameter

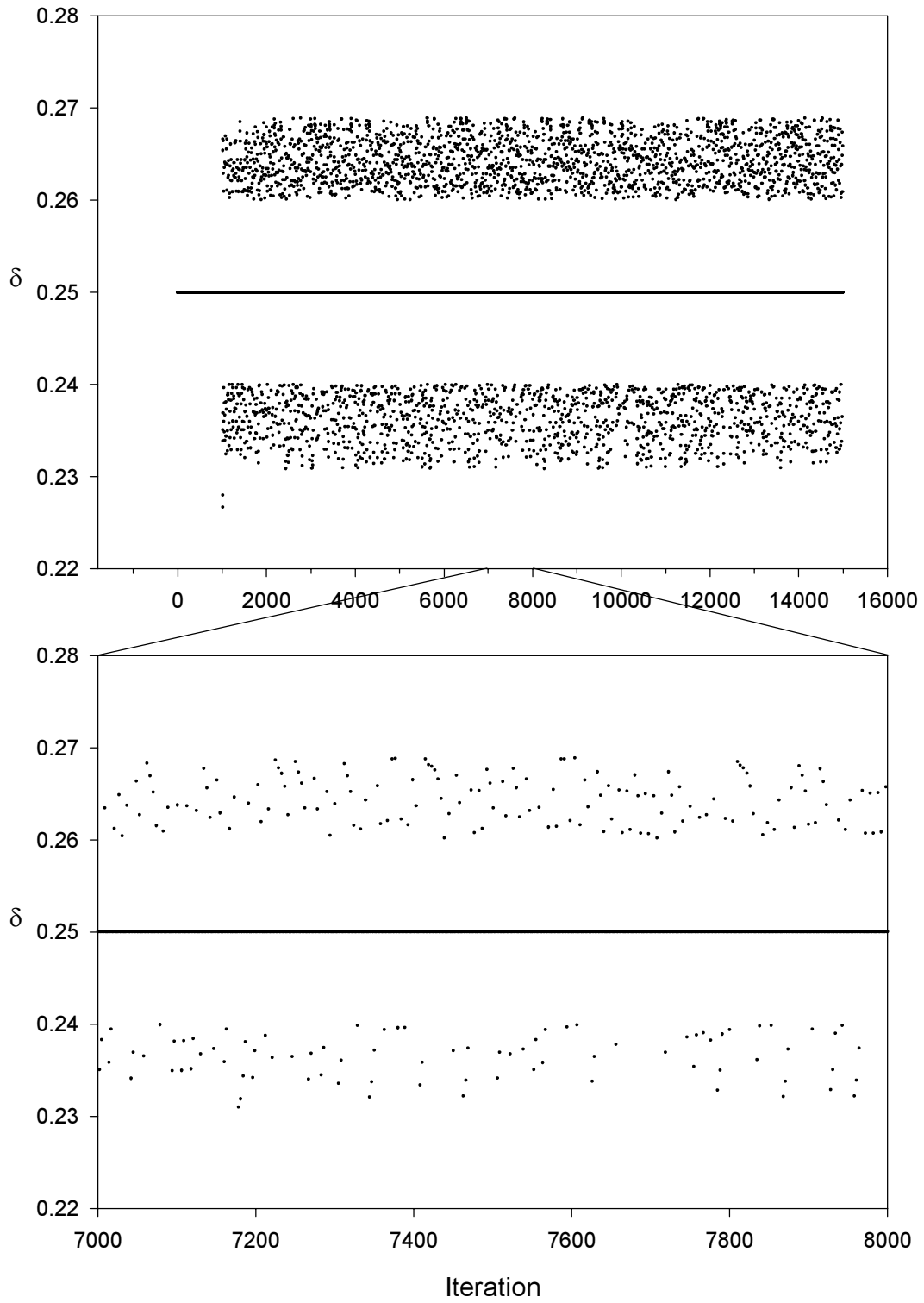


Figure 4.13: Scatter Plot of the Control Parameter at Each Iteration

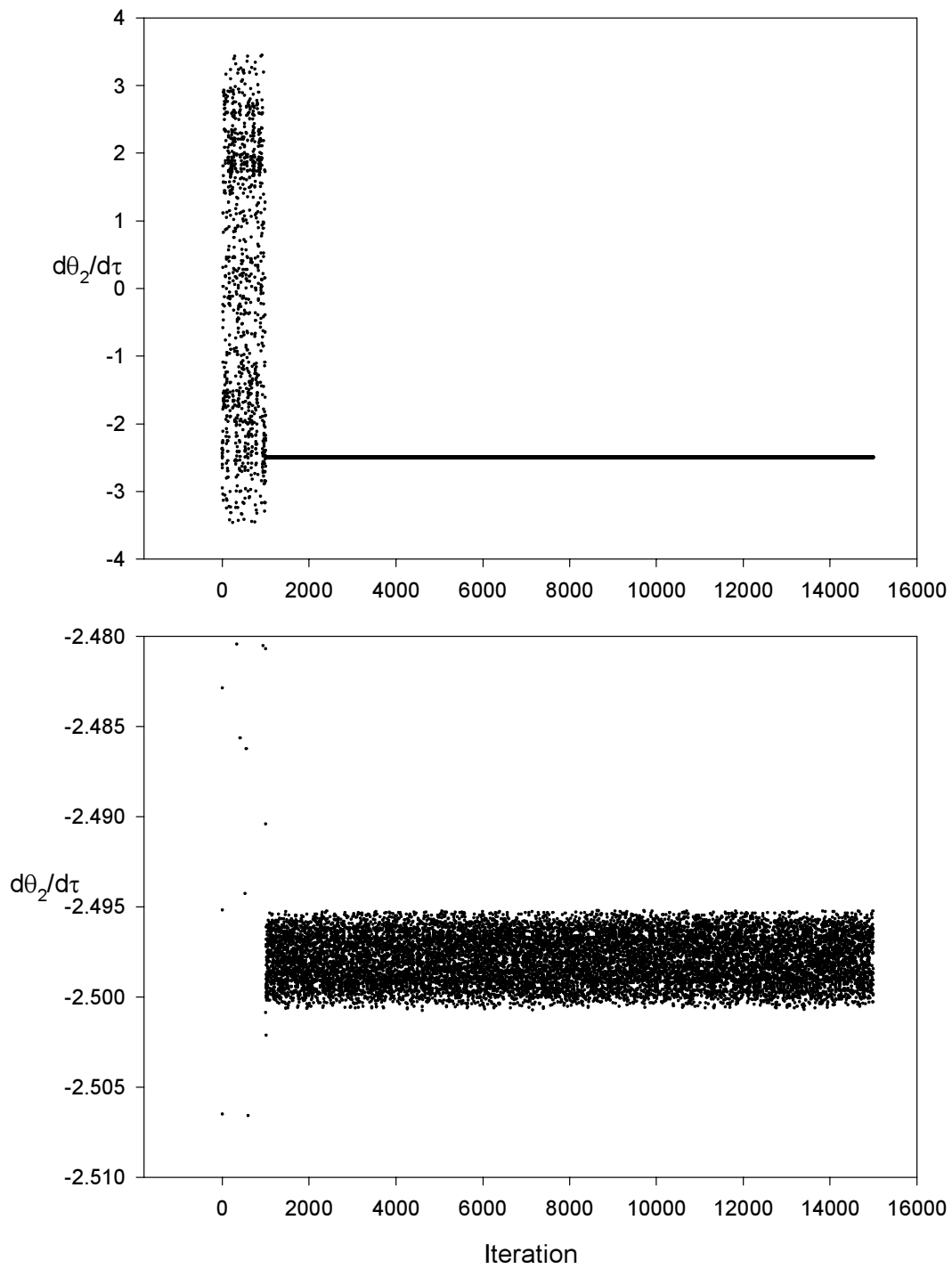


Figure 4.14: Control with Maximum and Discrete Value Restriction on the Control Parameter

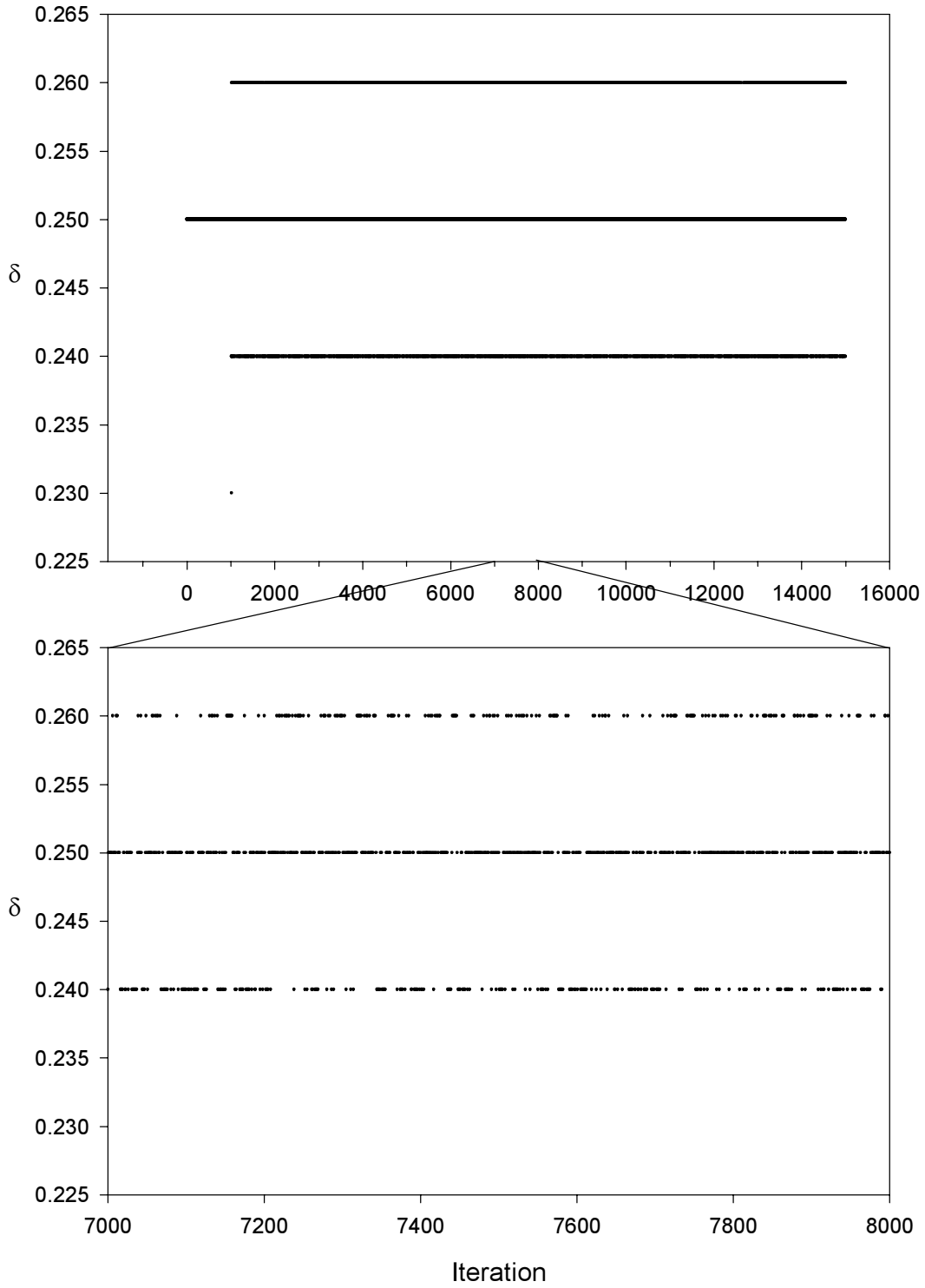


Figure 4.15: Scatter Plot of the Control Parameter at Each Iteration

Table 4.1: The Average Value and Standard Deviation of the Observable

Minimum or Step Size	Maximum and Minimum		Maximum and Discrete	
	Average	Standard Deviation	Average	Standard Deviation
1.0×10^{-3}	-2.497916	1.545643×10^{-4}	-2.497887	1.293553×10^{-4}
5.0×10^{-3}	-2.497902	7.299597×10^{-4}	-2.497875	6.528433×10^{-4}
1.0×10^{-2}	-2.497860	1.793826×10^{-3}	-2.497921	1.301090×10^{-3}
1.5×10^{-2}	-2.498080	3.098827×10^{-3}	-2.498008	1.962033×10^{-3}
2.0×10^{-2}	-2.498085	4.418207×10^{-3}	-2.498225	2.648088×10^{-3}
2.5×10^{-2}	—	—	-2.498343	3.288514×10^{-3}
3.0×10^{-2}	—	—	-2.498567	3.942095×10^{-3}

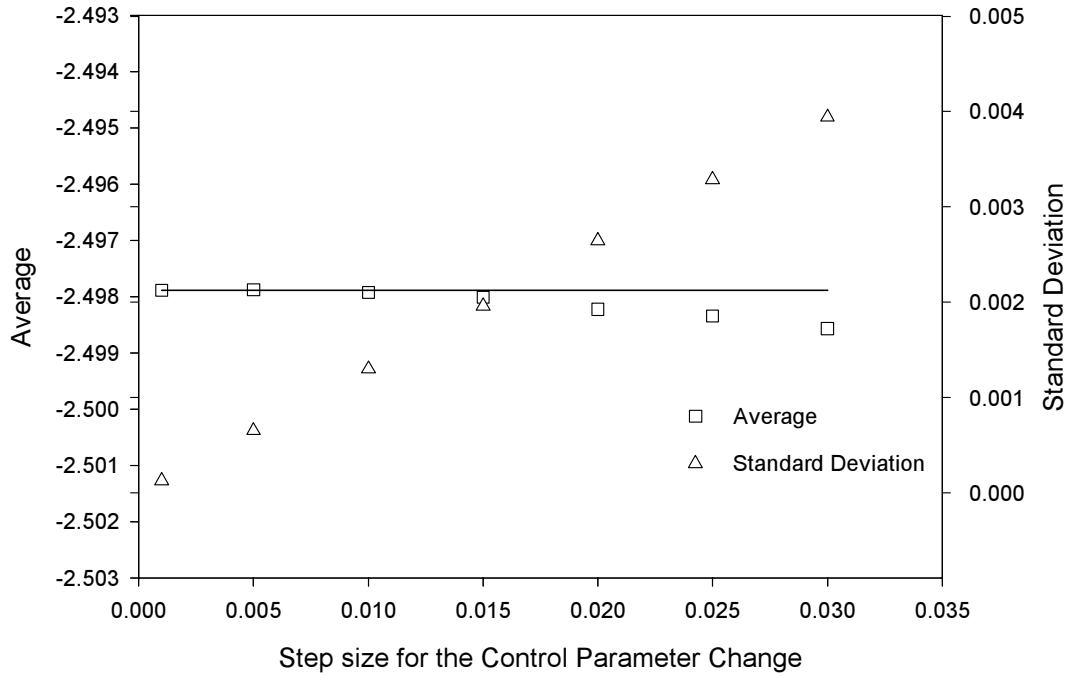
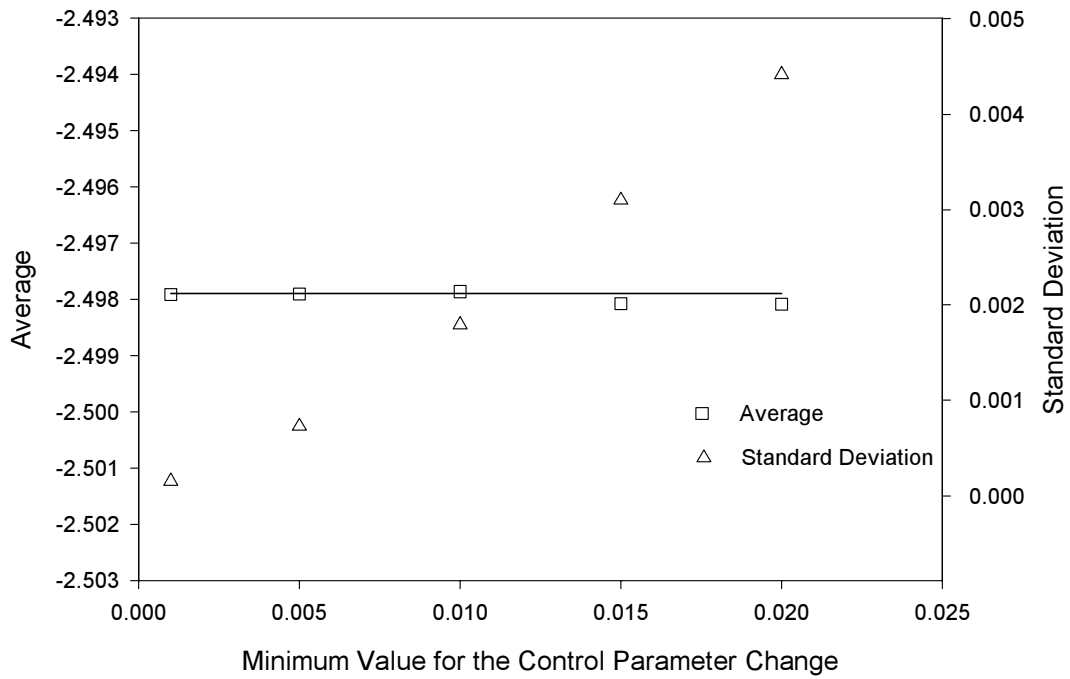


Figure 4.16: Average Values and Standard Deviations for Different Minimum Value for the Control Parameter Change (Top) and Different Step Size for the Control Parameter Change (Bottom)

is no number in the table for minimum restriction above 2.0×10^{-2} because the system could not be controlled under that condition.

4.5 Control Using Torque on the Lower Part of the Double Pendulum as the Control Parameter

One of the advantages of the OGY control scheme is that it is not restricted to a certain control parameter. All the control scheme requires is a system parameter that is available. In this section, the control is achieved by applying a small torque on the lower part of the double pendulum. For all cases in this section, the maximum allowable change of the control parameter is 5.0×10^{-2} . Figure 4.17 is the control with only a restriction on the maximum. Figure 4.18 is the plot of the control parameter at each iteration. Figure 4.19 shows the result of applying control with both the maximum and minimum restriction. The minimum restriction for the case shown is 5.0×10^{-3} . Figure 4.20 is the plot of control parameter at each iteration. Figure 4.21 and figure 4.22 are the control and parameter for the system with maximum and discrete restrictions. The step size for the discrete restriction is 5.0×10^{-3} for this case. Table 4.2 shows the average values and standard deviation of the observable motion. Figure 4.23 is the plot of the values in table 4.2. Again, the average values remain essentially the same while the standard deviations increase as the minimum or step size increases. Comparing the values in table 4.2 with those in table 4.1 under similar restriction suggests that torque can have a larger effect on the system. This is reasonable because the displacement of the base point affects the observable motion ($\dot{\theta}_2$) indirectly while torque affects it directly.

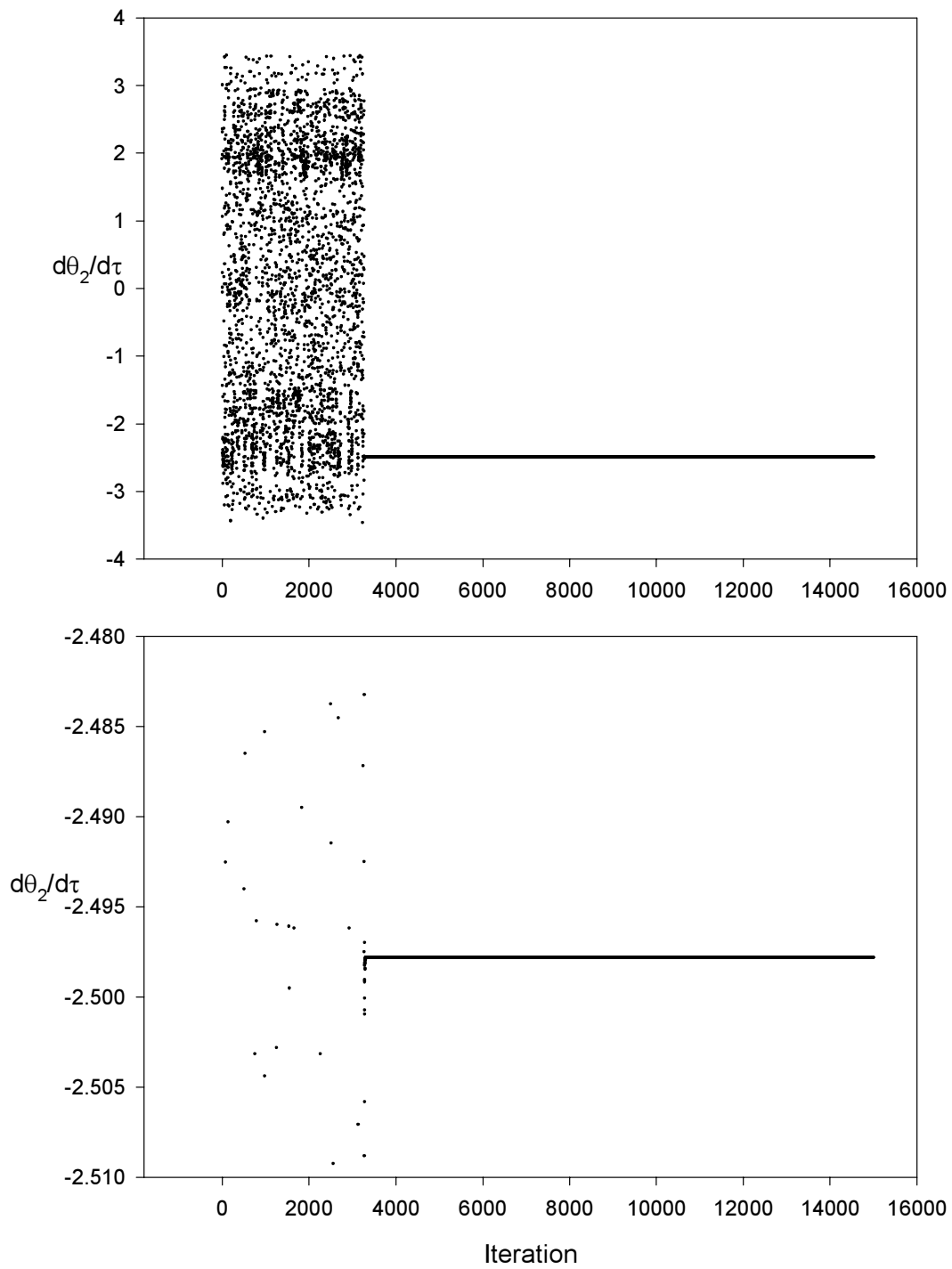


Figure 4.17: Control of the System with Only Maximum Restriction on the Control Parameter

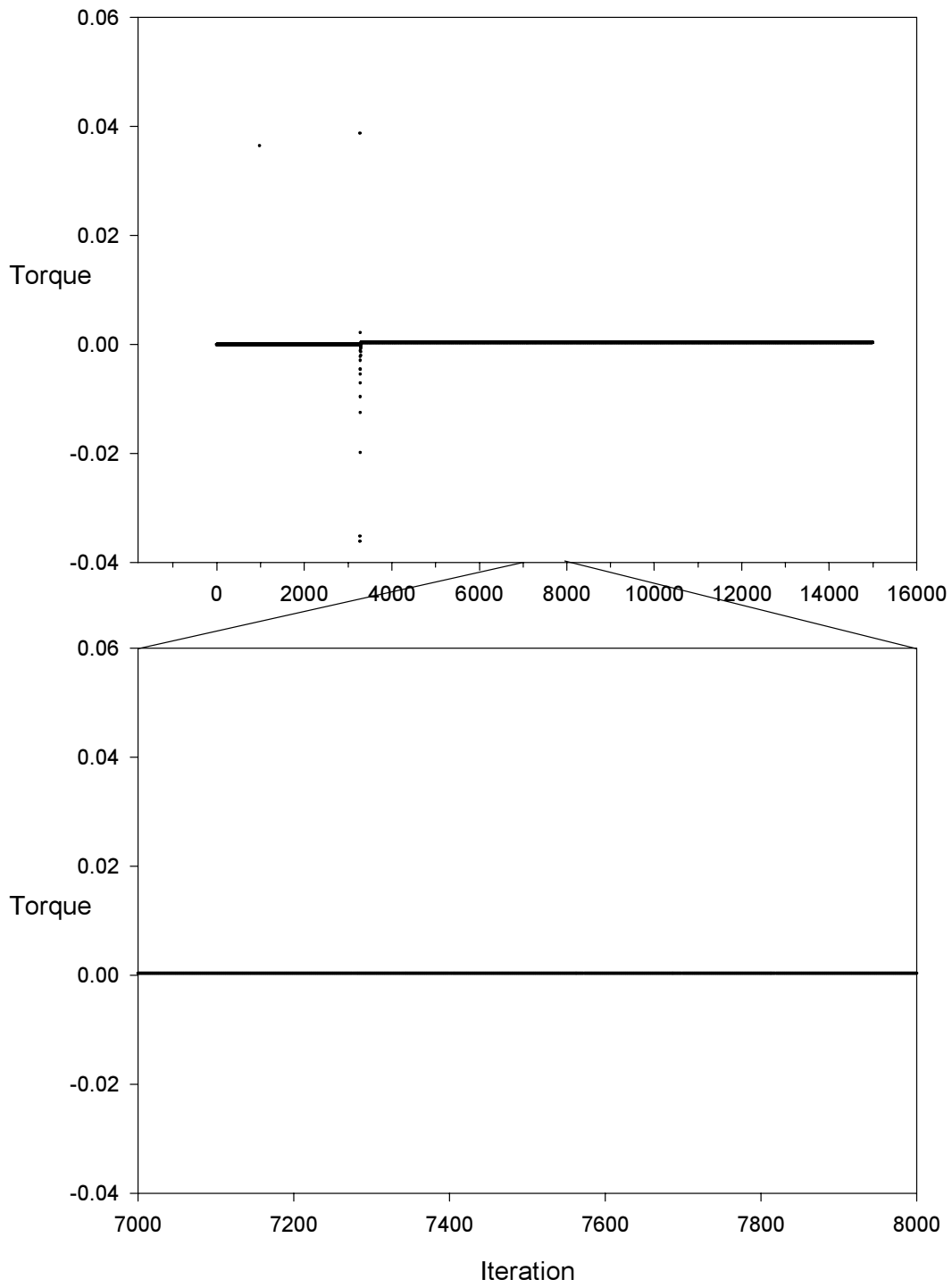


Figure 4.18: Scatter Plot of the Control Parameter at Each Iteration

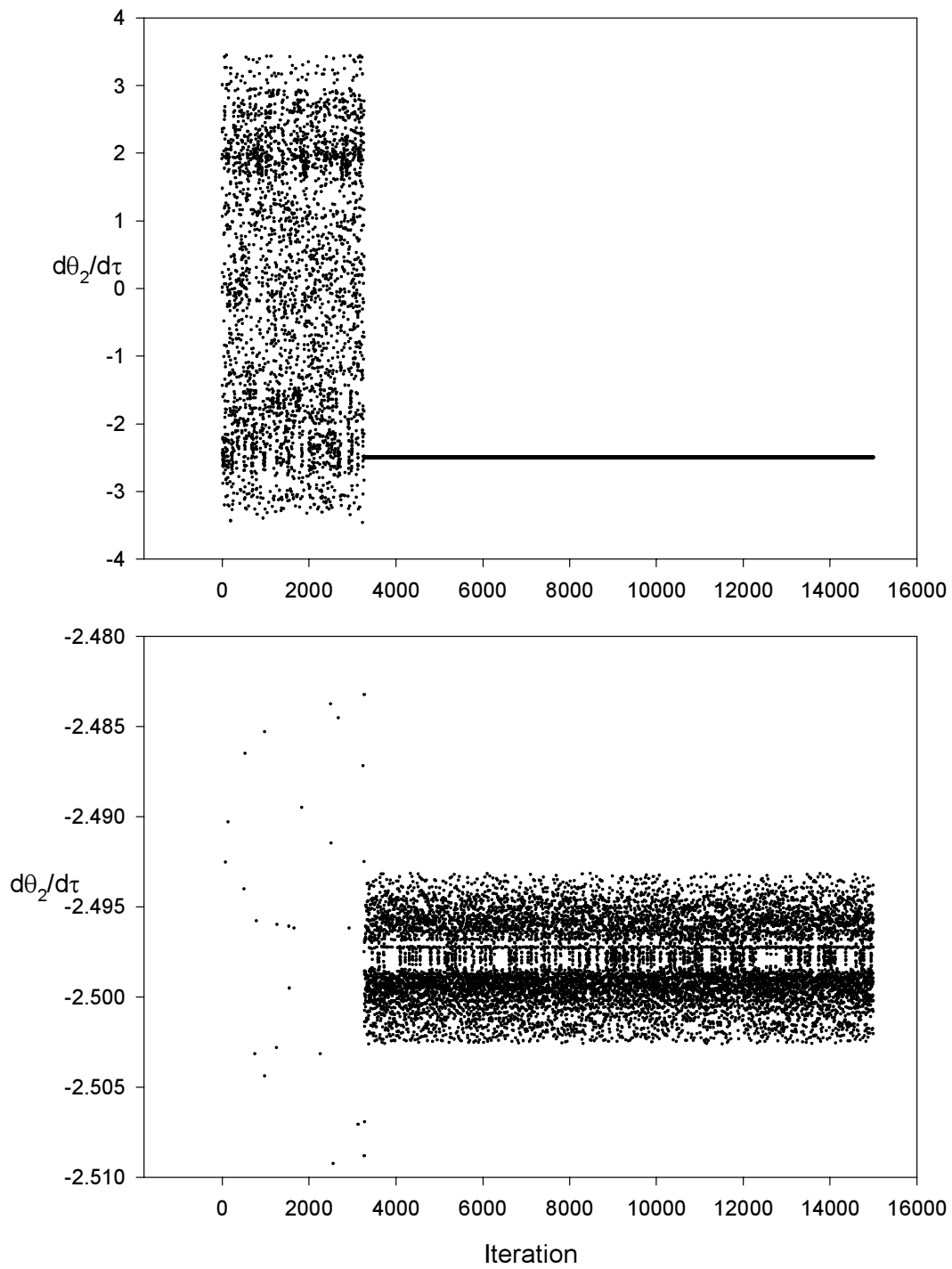


Figure 4.19: Control with Both Minimum and Maximum Restriction on the Control Parameter

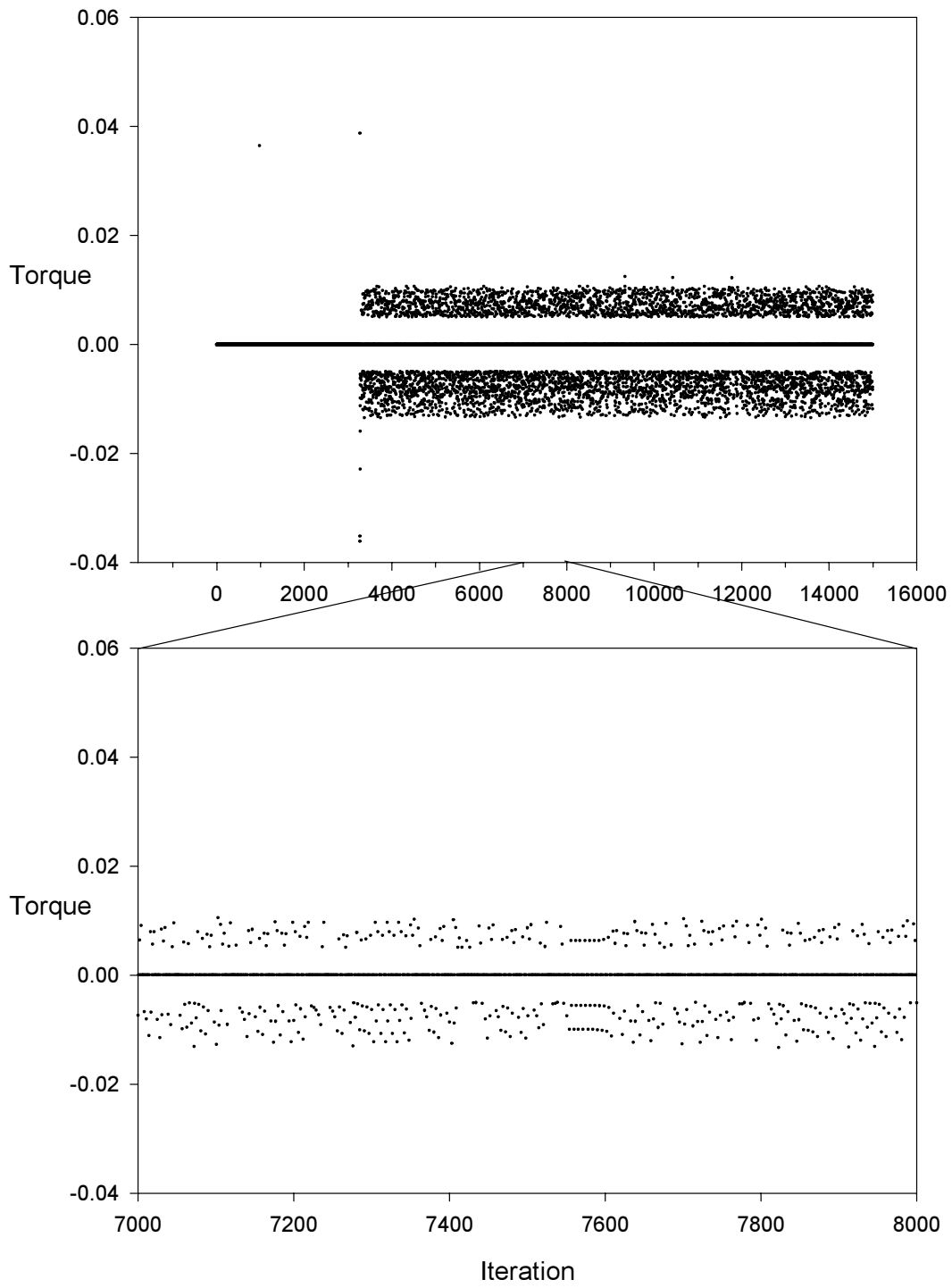


Figure 4.20: Scatter Plot of the Control Parameter at Each Iteration

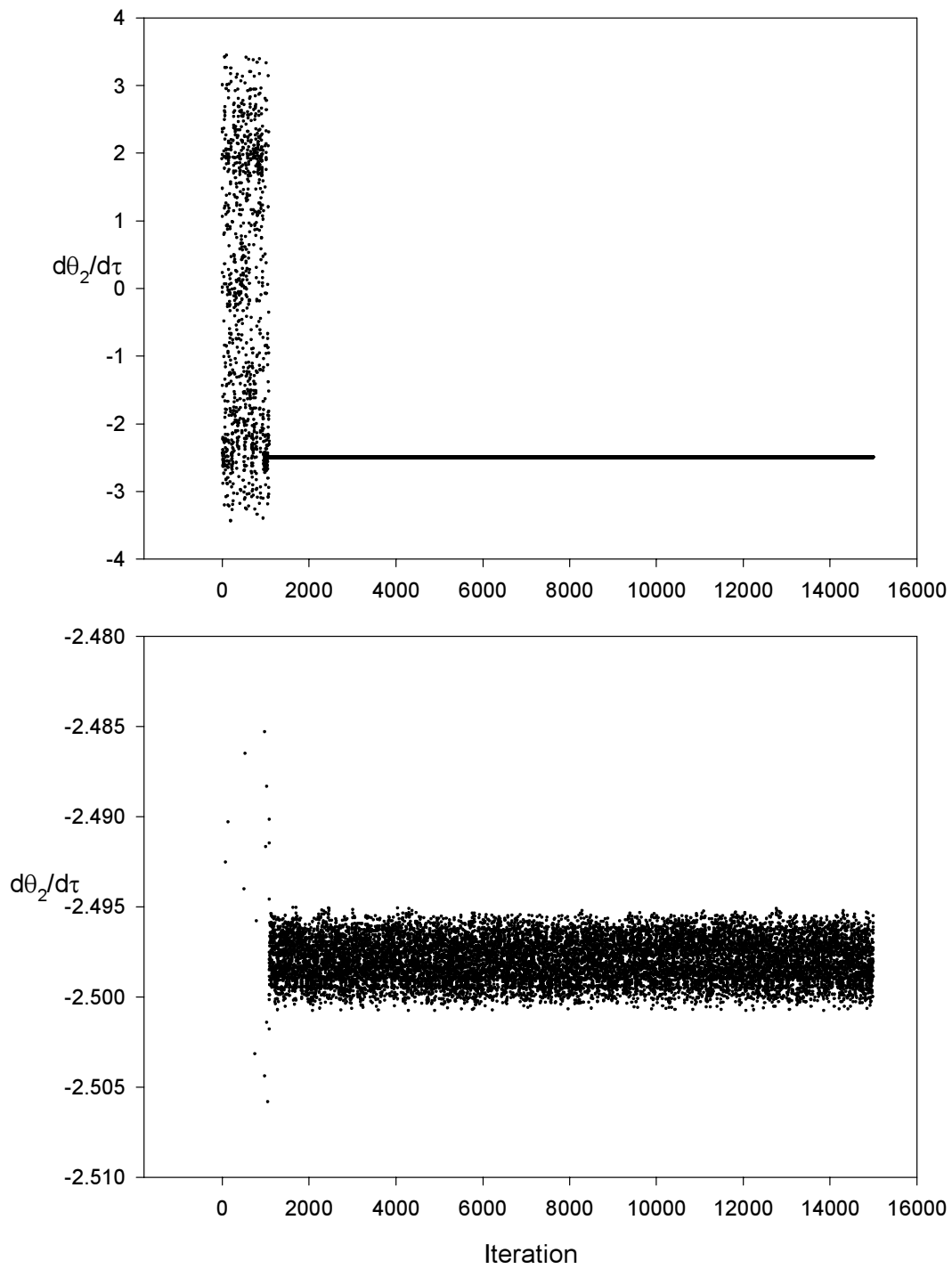


Figure 4.21: Control with Maximum and Discrete Value Restriction on the Control Parameter

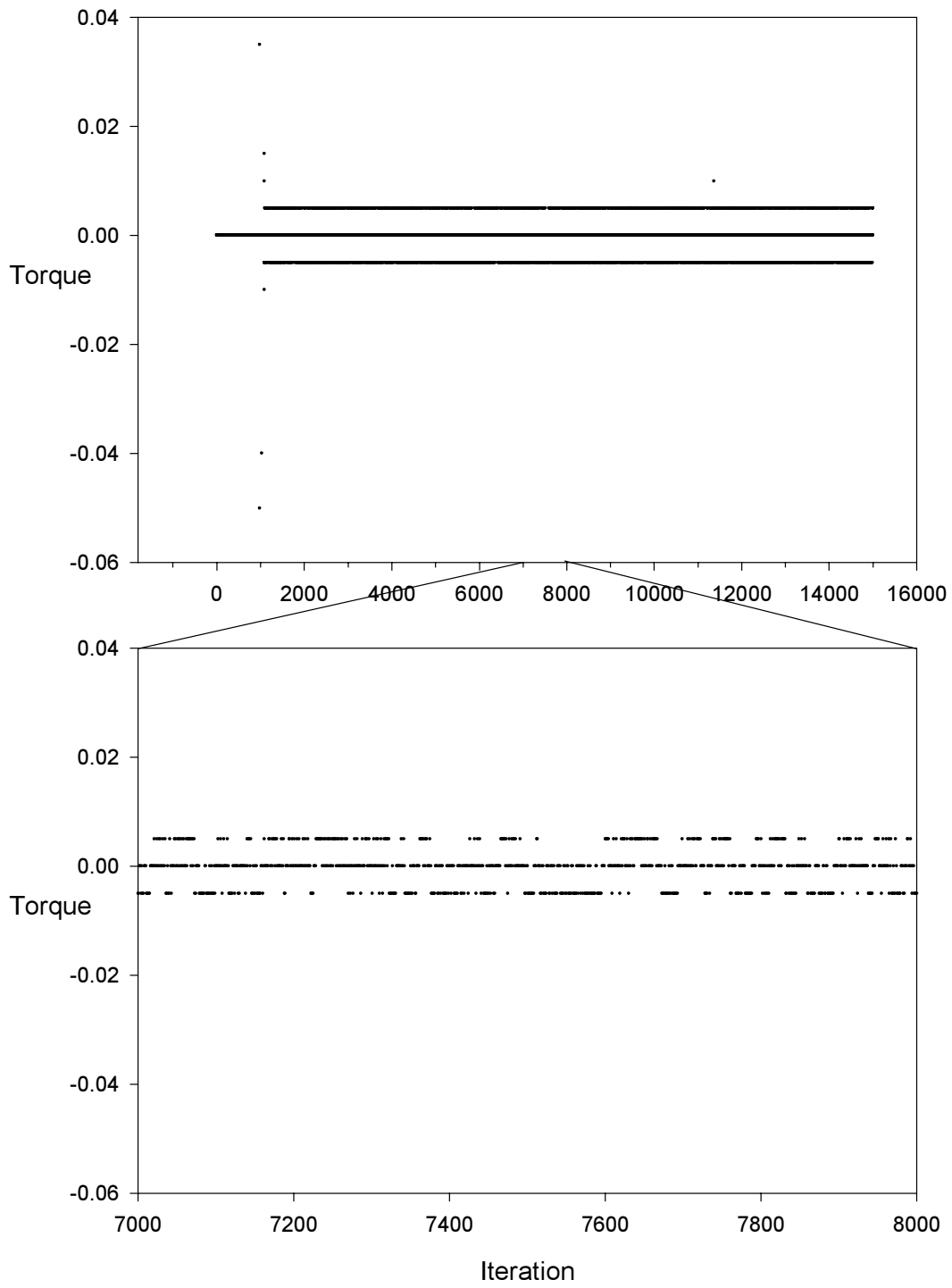


Figure 4.22: Scatter Plot of the Control Parameter at Each Iteration

Table 4.2: The Average Value and Standard Deviation of the Observable

Minimum or Step Size	Maximum and Minimum		Maximum and Discrete	
	Average	Standard Deviation	Average	Standard Deviation
1.0×10^{-3}	-2.497917	2.198235×10^{-4}	-2.497847	2.380706×10^{-4}
2.5×10^{-3}	-2.497885	5.962525×10^{-4}	-2.497878	5.859296×10^{-4}
5.0×10^{-3}	-2.498202	2.150118×10^{-3}	-2.497952	1.174405×10^{-3}
7.5×10^{-3}	-2.497955	3.081884×10^{-3}	-2.498104	1.790461×10^{-3}
1.0×10^{-2}	—	—	-2.498562	2.466325×10^{-3}

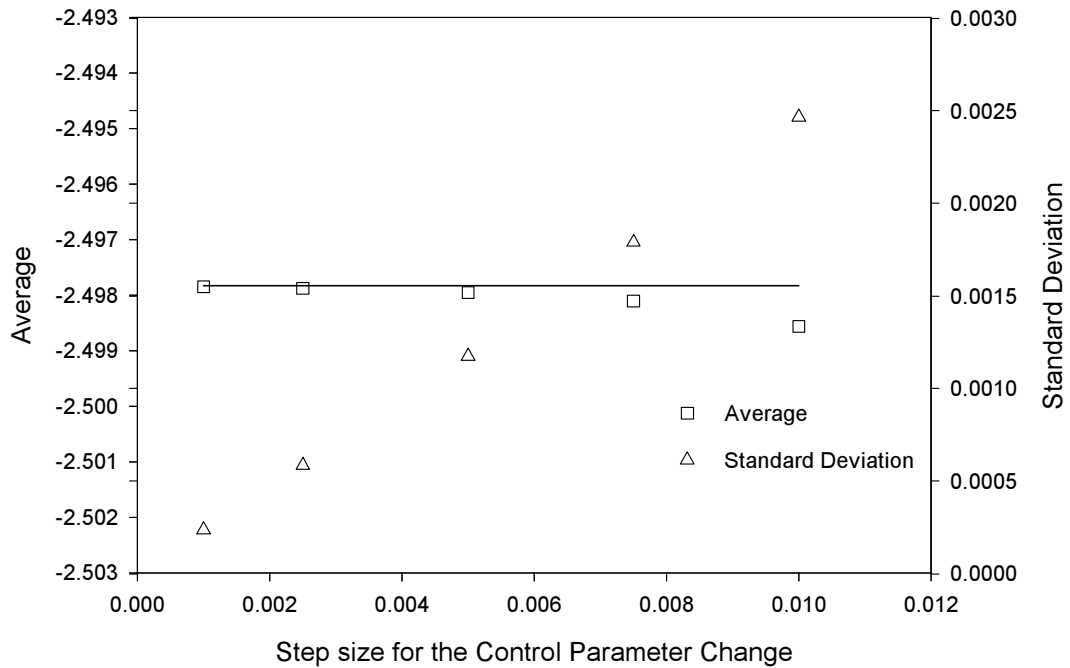
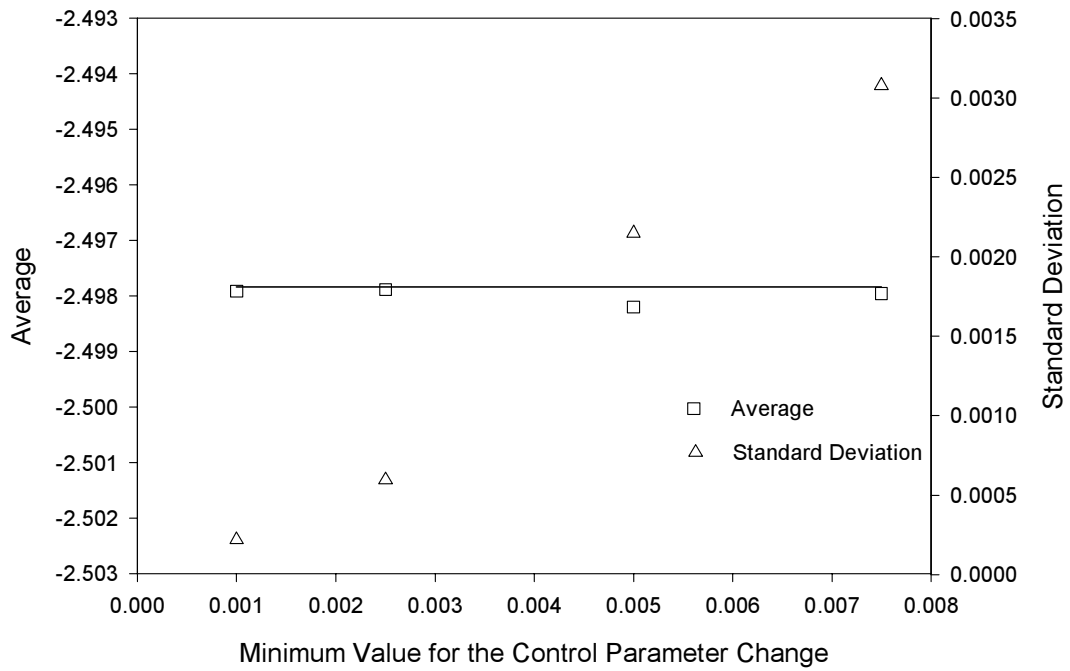


Figure 4.23: Average Values and Standard Deviations for Different Minimum Value for the Control Parameter Change (Top) and Different Step Size for the Control Parameter Change (Bottom)

4.6 The On-Off Control

In the previous two sections, it was shown that it is possible to maintain control by using a discrete set of control parameter changes. To push this idea to the limit, one can ask if it is possible to maintain control of the system by using only a minimum number of values for the parameter change. The simplest way is to use only three values, p_0 , $p_0 + \delta p$, and $p_0 - \delta p$, where p_0 is the nominal value of the control parameter and δp is a predefined value for the change of the parameter. This approach is called on-off control here because the controller has only three states, positive-on, off, and negative-on. This approach has two advantages. First, it simplifies the implementation of the controller. Second, it minimizes the time required to activate the control. Figure 4.24 shows the result of applying the on-off control on the system. The magnitude of the parameter change used for the figure is 5.0×10^{-3} . Figure 4.25 shows the control parameter at each iteration. Figure 4.26 to figure 4.28 show the plots of θ_1 , θ_2 , and $\dot{\theta}_1$. These plots indicate that the system is actually under control.

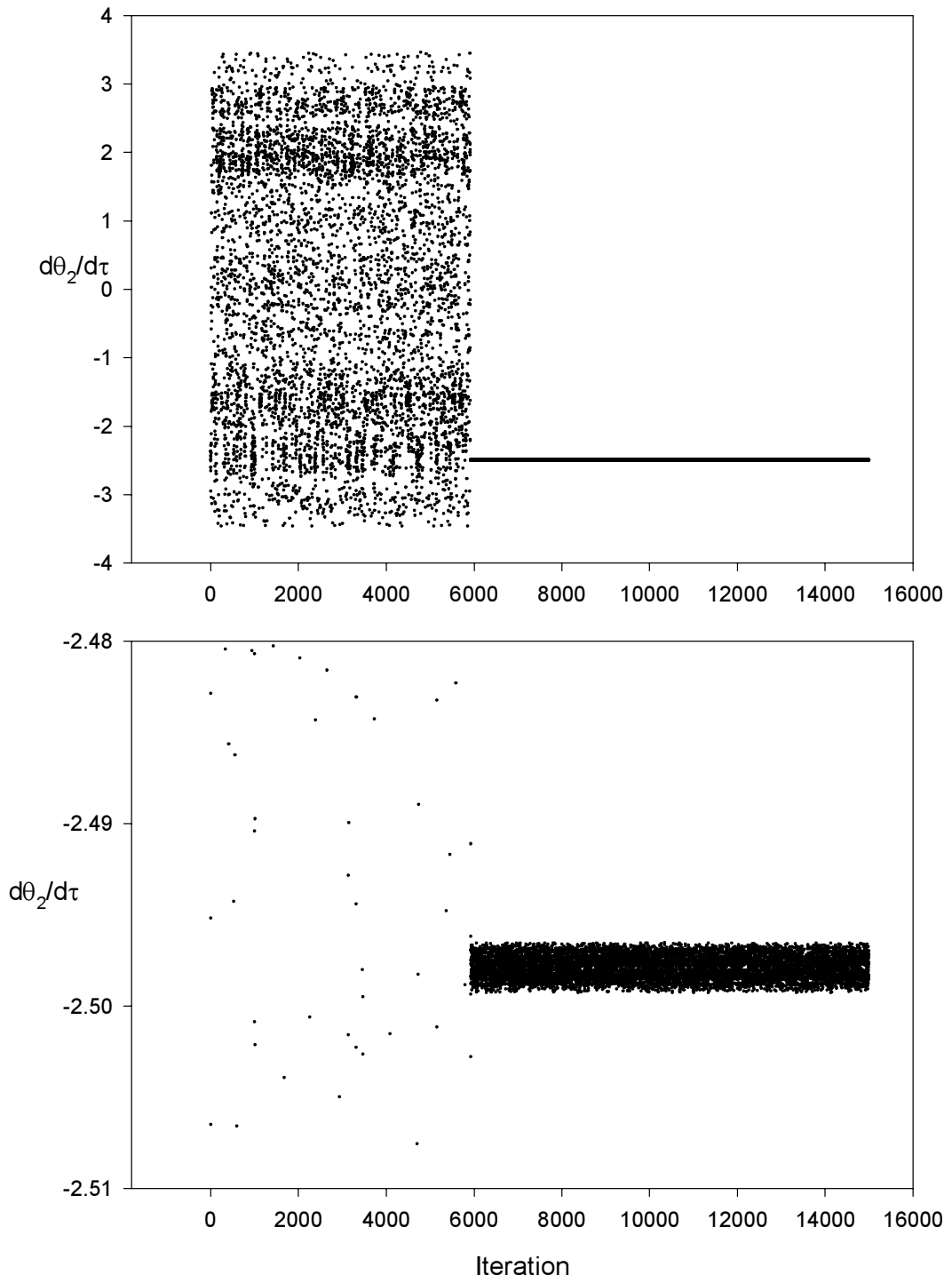


Figure 4.24: Control Using the On-Off Approach

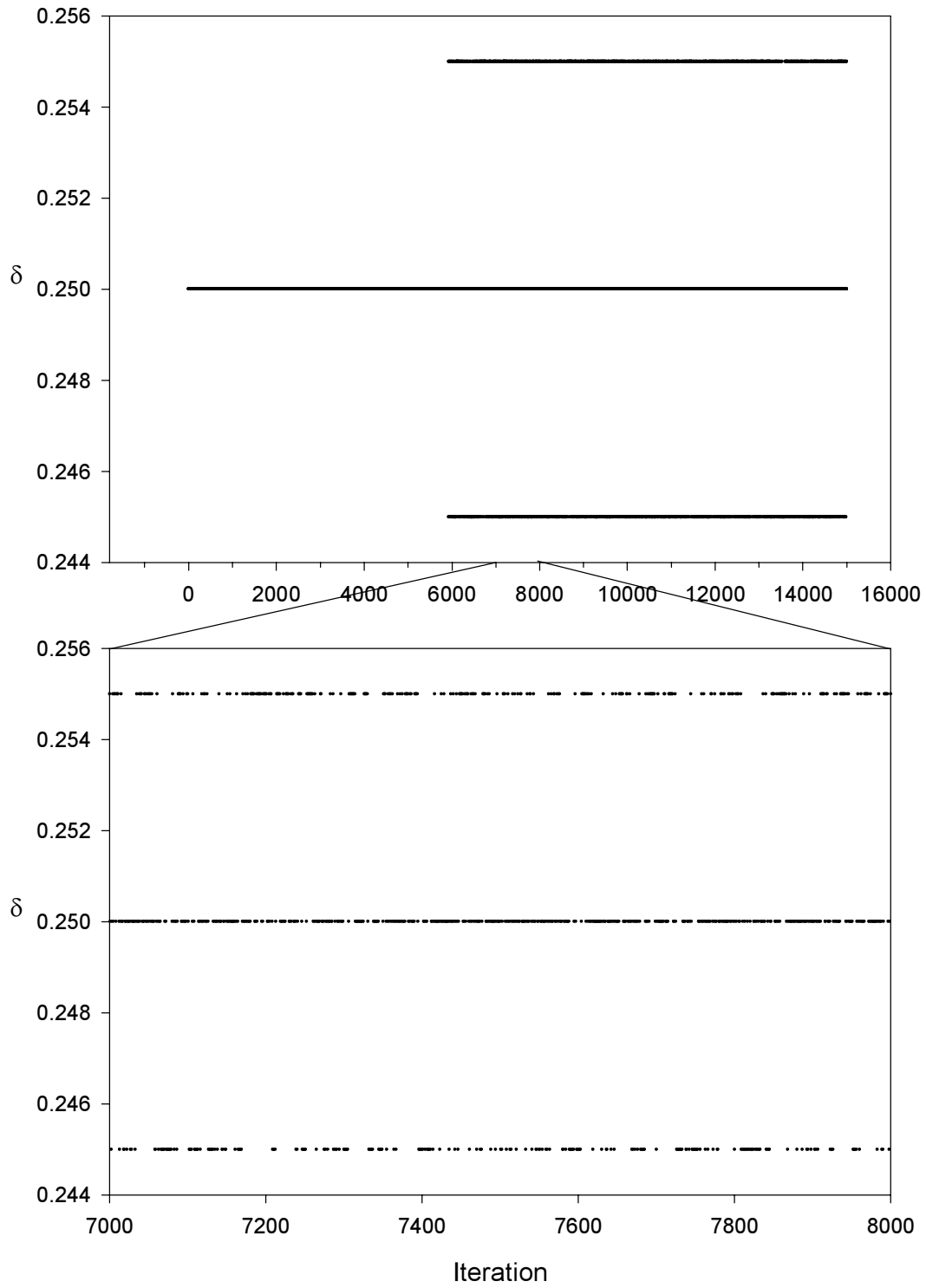


Figure 4.25: Scatter Plot of the Control Parameter at Each Iteration

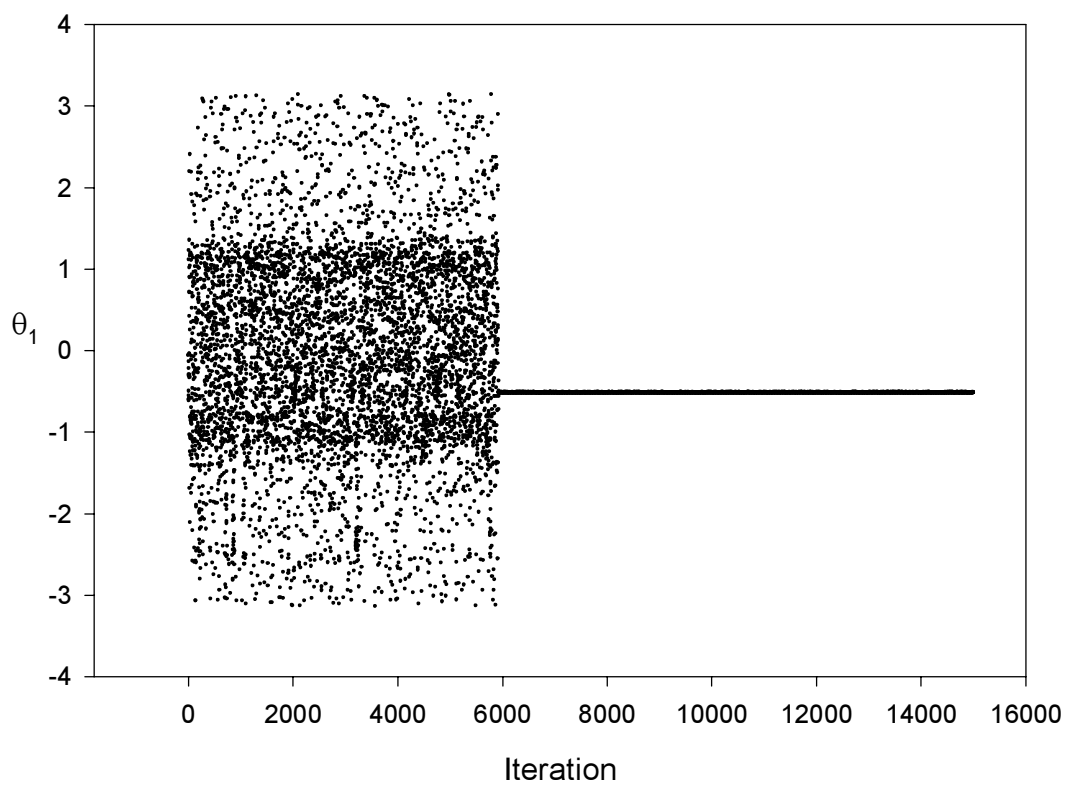


Figure 4.26: θ_1 at Each Iteration

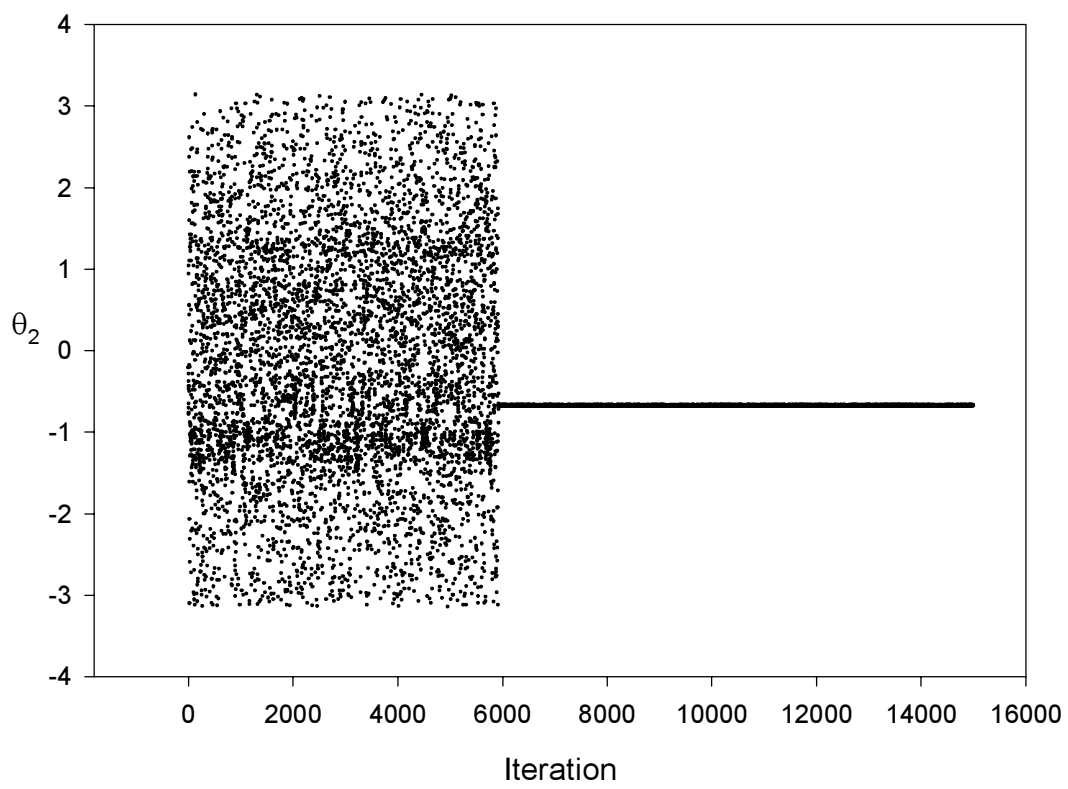


Figure 4.27: θ_2 at Each Iteration

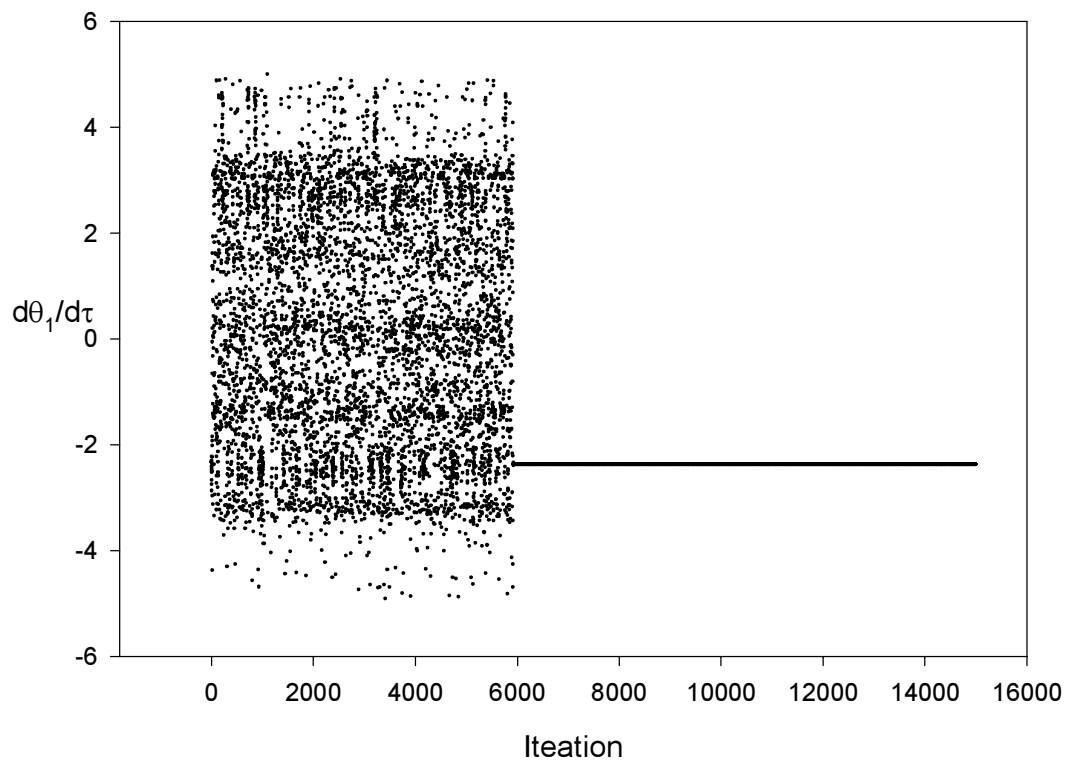


Figure 4.28: $\dot{\theta}_1$ at Each Iteration

Chapter 5

Conclusion and Future Work

5.1 Conclusion

When the chaos phenomenon was first discovered, there was a lot of excitement about it. Much of the earlier research concentrated on finding chaos in various systems. When researchers study nonlinear systems and encounter chaotic behavior, they typically modify their models to eliminate the chaotic behavior. These modifications are significant. More recently, researchers gained more insight into chaos and have included chaos in their control schemes. The OGY control scheme tries to utilize the infinite UPOs embedded in the strange attractor to stabilize the system. On the other hand, some researchers tried to make their system more chaotic to get better mixing between fuel and oxygen in an engine. There was some success in both directions.

This research has accomplished the following objectives:

1. Applied a newly developed method for locating UPO and further validated its usefulness.
2. Applied the higher dimensional extension of OGY control to a system that has not

been used before ¹.

3. Studied the effect of imposing minimum values for the change of the control parameter.
4. Studied the effect of using only discrete values for the change of the control parameter.
5. Proposed an on-off control scheme based on the higher-dimension extension of the OGY control method.

This research also shows that the OGY control scheme is not the best method for ship-mounted cranes. In order to use the OGY scheme, the system has to be in chaos. From numerical simulations, it is evident that the double pendulum will go over the top under that situation. Real cranes use cables instead of rigid massless bars and hence are more complicated. It is definitely possible that regions of chaos exist with relatively small pendulations ($\leq \frac{\pi}{2}$). But it might be better to use other control schemes in that situation. Besides, the target state of the OGY control is a fixed point on the Poincaré map which is in fact a periodic motion. The desired control state for a ship-mounted crane is an actual fixed point.

5.2 Future Work

There are two areas for future work, application and performance. Although it is shown that OGY is not the best control strategy for the ship-mounted crane, there might be systems that are more suitable for this scheme. It is important to identify these systems and try to apply the control scheme on them. On the performance side, more study should be made to shorten the transient before the activation of control. The other issues that should receive consideration are noise and time-delay for the application of the control. In a real system, noise will always be present. Studies should be done to determine the effect of noise on

¹Christini, Collins, and Linsay [9] applied a quasi-continuous control to a double pendulum. But the external excitation for the system is a torque at the base point, which leads to simpler equations of motion than those investigated in this research.

the control. Since the system will not be able apply the control instantly as in a numerical simulation, the effect of this delay should also be studied.

Bibliography

- [1] H. D. I. Abarbanel. *Analysis of Observed Chaotic Data*. Springer-Verlag, New York Berlin Heidelberg, 1996.
- [2] H. D. I. Abarbanel, R. Brown, J. L. Sidorowich, and L. Sh. Tsimring. The analysis of observed chaotic data in physical systems. *Rev. Mod. Phys.*, 65:1331–1392, 1993.
- [3] P. M. Alsing, A. Gavrielides, and V. Kovanis. Using neural networks for controlling chaos . *Phys. Rev. E*, 49(2):1225–1231, 1994.
- [4] J. Alvarez-Ramírez. Nonlinear feedback for controlling the Lorenz equation. *Phys. Rev. E*, 50(3):2339–2342, 1994.
- [5] D. Auerbach, C. Grebogi, E. Ott, and J. Yorke. Controlling chaos in high dimensional systems. *Phys. Rev. Lett.*, 69:3479–3482, 1992.
- [6] P. E. Bak, R. Yoshino, N. Asakura, and T. Nakano. Identification of unstable periodic orbit in inter-edge-localized-mode intervals in jt-60u. *Physical Review Letters*, 83(7):1339–1342, 1999.
- [7] E. Barreto and C. Grebogi. Multiparameter control of chaos. *Phys. Rev. E*, 52(4):3553–3557, 1995.
- [8] S. Boccaletti, A. Farini, E. J. Kostelich, and F. T. Arecchi. Adaptive targeting of chaos. *Phys. Rev. E*, 55(5):4845–4848, 1997.

- [9] D. J. Christini, J. J. Collins, and P. S. Linsay. Experimental control of high-dimensional chaos: The driven double pendulum. *Phys. Rev. E*, 54(5):4824–4827, 1996.
- [10] R. L. Devaney. *An Introduction to Chaotic Dynamical Systems*. Addison-Wesley, Reading Mass., 1989.
- [11] M. Ding, Yang. W., V. In, W. L. Ditto, M. L. Spano, and B. Gluckman. Controlling chaos in high dimensions: theory and experiment. *Phys. Rev. E*, 53(5):4334–4344, 1996.
- [12] W. L. Ditto, S. N. Rauseo, and M. L. Spano. Experimental control of chaos. *Phys. Rev. Lett.*, 65:3211–3214, 1990.
- [13] E. J. Doedel. AUTO: A program for the automatic bifurcation analysis of autonomuos systems. In *Proc. 10th Manitoba Conf. Num. Math. and Comp. Winnipeg, Canada*, pages 265–284, 1981.
- [14] U. Dressler and G. Nitsche. Controlling chaos using time delay coordinates. *Phys. Rev. Lett.*, 68:1–4, 1992.
- [15] J.-P. Eckmann, S. O. Kamphorst, D. Ruelle, and S. Ciliberto. Liapunov exponents from time series. *Phys. Rev. A*, 34:4971–4979, 1986.
- [16] L. Flepp, R. Holzner, E. Brun, and M. Finardi R. Badii. Model identification by periodic-orbit analysis from NMR-laser chaos. *Phys. Rev. Lett.*, 67:2244, 1991.
- [17] A. Garfinkel, M. L. Spano, W. L. Ditto, and J. N. Weiss. Controlling cardiac chaos. *Science*, 257:1230–1235, 1992.
- [18] Z. Gills, C. Iwata, R. Roy, Schwartz I., and I. Triandaf. Tracking unstable steady states: extending the stability regime of a multimode laser system. *Phys. Rev. Lett.*, 69:3169–3172, 1992.
- [19] C. Grebogy, J. A. Yorke, E. Ott, and B. Hunt. Control of shipboard cranes. In *Proc. Kick-Off Meeting: MURI-Nonlinear Active Control of Dynamical Systems*, 1996.

- [20] J. Guckenheimer and P. J. Holmes. *Nonlinear oscillations, dynamical systems, and bifurcations of vector fields*. Springer-Verlag, Berlin, 1983.
- [21] R. Hegger, H. Kantz, and T. Schreiber. Practical implementation of nonlinear time series methods: The TISEAN package. *Chaos*, 9(2):413–435, 1999.
- [22] P. J. Holmes. A nonlinear oscillator with a strange attractor. *Phil. Trans. Roy. Soc. London*, 292:419–448, 1979.
- [23] A. Hübler and E. Lüscher. Resonant stimulation and control of nonlinear oscillators. *Naturwissenschaften*, 76:67–69, 1989.
- [24] E. R. Hunt. Stabilizing high period orbits in a chaotic system: The diode resonator. *Phys. Rev. Lett.*, 67:1953–1955, 1991.
- [25] H. Kantz. A robust method to estimate the maximal Lyapunov exponent of a time series. *Phys. Lett. A*, 185:77–87, 1994.
- [26] H. Kantz and Th. Schreiber. *Nonlinear Time Series Analysis*. Cambridge Univ. Press, Cambridge, UK, 1997.
- [27] M. B. Kennel, R. Brown, and H. D. I. Abarbanel. Determining embedding dimension for phase-space reconstruction using a geometrical construction. *Phys. Rev. A*, 45:3403–3411, 1992.
- [28] E. Kostelich, C. Grebogi, E. Ott, and J. A. Yorke. Higher-dimensional targeting. *Phys. Rev. E*, 47:305–310, 1993.
- [29] W. Lacarbonara, R. Soper, Z. Masoud, J. Pratt, and Ali H. Nayfeh. Towards a hybrid variable-geometry-truss architecture for pendulation control in ship-mounted cranes. In *Proc. Third Semi-Annual Meeting: MURI-Nonlinear Active Control of Dynamical Systems*, 1998.

- [30] Y-Ch. Lai, M. Ding, and C. Grebogi. Controlling Hamiltonian chaos. *Phys. Rev. E*, 47:86–90, 1993.
- [31] D. P. Lathrop and E. J. Kostelich. Characterization of an experimental strange attractor by periodic orbits. *Phys. Rev. A*, 40:4028–4031, 1989.
- [32] E. N. Lorenz. Deterministic nonperiodic flow. *J. Atmos. Sci.*, 20:130–141, 1963.
- [33] J. B. McLaughlin. Period-doubling bifurcations and chaotic motion for a parametrically forced pendulum. *J. Stat. Phys.*, 24:375, 1981.
- [34] F. C. Moon and P. J. Holmes. A magnetoelastic strange attractor. *J. Sound Vib.*, 65(2):285–296, 1979.
- [35] Francis C. Moon. *Chaotic Vibration*. John Wiley & Sons, 1987.
- [36] A. H. Nayfeh. *Introduction to perturbation techniques*. Wiley & Sons, New York, 1981.
- [37] A. H. Nayfeh and D. T. Mook. *Nonlinear Oscillations*. John Wiley & Sons, New York, Chichester, Brisbane, Toronto, 1979.
- [38] G. Nitsche and U. Dressler. Controlling chaotic dynamical systems using time delay coordinates. *Physica D*, 58:153–164, 1992.
- [39] E. Ott. *Chaos in Dynamical Systems*. University Press, Cambridge, 1993.
- [40] E. Ott, C. Grebogi, and J. A. Yorke. Controlling chaos. *Phys. Rev. Lett.*, 64:1196–1199, 1990.
- [41] E. Ott, T. Sauer, and J. A. Yorke, editors. *Coping with chaos; Analysis of chaotic data and the exploitation of chaotic systems*. Wiley & Sons Inc., New Yorke, 1994.
- [42] N. H. Packard, J. P. Crutchfield, J. D. Farmer, and R. S. Shaw. Geometry from a time series. *Phys. Rev. Lett.*, 45:712–716, 1980.

- [43] T. S. Parker and L. O. Chua. INSITE. A software toolkit of the analysis of nonlinear dynamical systems. *Proc. IEEE*, 75, 1987.
- [44] T. S. Parker and L. O. Chua. *Practical numerical algorithms for chaotic systems*. Springer-Verlag, Berlin, 1989.
- [45] V. Petrov, V. Gáspár, J. Masere, and K. Showalter. Controlling chaos in the Belousov-Zhabotinsky reaction. *Nature*, 361:240–243, 1993.
- [46] H. Poincaré. *Les méthodes nouvelles de la mécanique céleste*, volume 3. Gauthier-Villars, Paris, 1899.
- [47] K. Pyragas. Continuous control of chaos, by self-controlling feedback. *Phys. Lett. A*, 170:421–428, 1992.
- [48] K. Pyragas. Experimental control of chaos by delayed self-controlling feedback. *Phys. Lett. A*, 180:99–102, 1993.
- [49] S. Neil Rasband. *Chaotic Dynamics of Nonlinear Systems*. John Wiley & Sons, 1990.
- [50] C. Reyl, L. Flepp, R. Badii, and E. Brun. Control of NMR-laser chaos in high-dimensional embedding space. *Phys. Rev. E*, 47:267–272, 1993.
- [51] F. J. Romeiras, C. Grebogi, E. Ott, and W. P. Dayawansa. Controlling chaotic dynamical systems. *Physica D*, 58:165–192, 1992.
- [52] Michael T. Rosenstein, James J. Collins, and Carlo J. De Luca. A practical method for calculating largest Lyapunov exponents from small data sets. *Physica D*, 65:117–134, 1993.
- [53] R. Roy, T. D. Murphy Jr., T. D. Maier, Z. Gills, and E. R. Hunt. Dynamical control of a chaotic laser: experimental stabilization of a globally coupled system. *Phys. Rev. Lett.*, 68:1259–1262, 1992.

- [54] M. Sano and Y. Sawada. Measurement of Lyapunov spectrum from a chaotic time series. *Phys. Rev. Lett.*, 55:1082–1085, 1985.
- [55] C. G. Schroer, B. Hunt, E. Ott, J. A. Yorke, and G. Yuan. Targeting in chaotic system. In *Proc. First Semi-Annual Meeting: MURI-Nonlinear Active Control of Dynamical Systems*, 1997.
- [56] T. Shinbrot. Progress in the control of chaos. *Advan. Phys.*, 44(2):73–111, 1995.
- [57] T. Shinbrot, C. Grebogi, E. Ott, and J. A. Yorke. Using chaos to target stationary states of flows. *Phys. Lett. A*, 165:349–354, 1992.
- [58] P. So, E. Ott, T. Sauer, B. J. Gluckman, C. Grebogi, and St. J. Schiff. Extracting unstable periodic orbits from chaotic time series data. *Phys. Rev. E*, 55(5):5398–5417, 1997.
- [59] P. So, E. Ott, S. J. Schiff, D. T. Kaplan, T. Sauer, and C. Grebogi. Detecting unstable periodic orbits in chaotic experimental data. *Phys. Rev. Lett.*, 76(25):4705–4708, 1996.
- [60] Paul So, Joseph T. Francis, Theoden I. Netoff, Bruce J. Gluckman, and Steven J. Schiff. Periodic orbits: A new language for neuronal dynamics. *Biophysical Journal*, 74:2776–2785, 1998.
- [61] J. Starrett and R. Tagg. Control of a chaotic parametrically driven pendulum. *Phys. Rev. Lett.*, 74(11):1974–1977, 1995.
- [62] F. Takens. Detecting strange attractors in turbulence. In D. A. Rand and L.-S. Young, editors, *Dynamical Systems and Turbulence (Warwick 1980)*, volume 898 of *Lecture Notes in Mathematics ISBN 3 540 11171 9 and 0 387 11171 9*, pages 366–381. Springer-Verlag, Berlin, 1980.
- [63] Y. Ueda. Randomly transitional phenomena in the system governed by Duffing’s equation. *J. Stat. Phys.*, 20:181–190, 1979.

- [64] A. Wolf, J. B. Swift, H. L. Swinney, and J. A. Vastano. Determining Lyapunov exponents from a time series. *Physica D*, 16:285–317, 1985.

Appendix A

Equations of Motion in First Order Form

In order to use the IMSL library to integrate these equations, it is necessary to convert the equations of motion into first order differential equations. This can be accomplished by defining $x'_1 = x_3$ and $x'_2 = x_4$ and the two equations of motion can be converted to

$$x'_1 = x_3$$

$$x'_2 = x_4$$

$$\begin{aligned} x'_3 = & -\frac{1}{l(m \cos^2(x_1 - x_2) - 1)} \left[-ml \cos(x_1 - x_2) \sin(x_1 - x_2) x_3^2 - \frac{m}{l} \mu_1 x_3 \right. \\ & - m\mu_2 \cos(x_1 - x_2) x_3 + \delta \tilde{\omega}_1^2 \cos \tilde{\omega}_1 \tau \cos x_1 + m\mu_2 x_4 \cos(x_1 - x_2) \\ & - m\delta \tilde{\omega}_1^2 \cos \tilde{\omega}_1 \tau \cos(x_1 - x_2) \cos x_2 - \eta \tilde{\omega}_2^2 \cos \tilde{\omega}_2 \tau \sin x_1 - \sin x_1 \\ & - mx_4^2 \sin(x_1 - x_2) + m \cos(x_1 - x_2) \sin x_2 \\ & \left. + m\eta \tilde{\omega}_2^2 \cos \tilde{\omega}_2 \tau \cos(x_1 - x_2) \sin x_2 \right] \end{aligned}$$

$$\begin{aligned}
x_4' = & -\frac{1}{1 - m \cos^2(x_1 - x_2)} \{ -l \sin(x_1 - x_2) x_3^2 + \mu_2(x_4 - x_3) \\
& - \delta \tilde{\omega}_1^2 \cos \tilde{\omega}_1 \tau \cos x_2 - l \cos(x_1 - x_2) \left[\frac{m \sin(x_1 - x_2) x_4^2}{l} + \frac{m}{l^2} \mu_1 x_3 \right. \\
& \left. - \frac{\delta}{l} \tilde{\omega}_1^2 \cos \tilde{\omega}_1 \tau \cos x_1 + \frac{\eta}{l} \tilde{\omega}_2^2 \cos \tilde{\omega}_2 \tau \sin x_1 + \frac{\sin x_1}{l} \right] \\
& \left. + \eta \tilde{\omega}_2^2 \cos \tilde{\omega}_2 \tau \sin x_2 + \sin x_2 \right\}.
\end{aligned}$$

Appendix B

Validation of the Fixed Point Transformation Method

B.1 Logistic Map

The logistic map is defined by the following equation:

$$x_{n+1} = f(x_n) = rx_n(1 - x_n).$$

The fixed points of the logistic map can be calculated by setting $x_{n+1} = x_n = x^*$ in the equation and solve for x^*

$$x^* = 0, \frac{r-1}{r}.$$

The Jacobian of the logistic map at x can be obtained by differentiation of the map with respect to x

$$\frac{df(x)}{dx} = r - 2rx.$$

The Jacobian can also be obtained from the iterated data set using the following approximate equation:

$$\frac{df}{dx}(x_n) \approx \frac{x_n - x_{n+1}}{x_{n-1} - x_n}.$$

Figure B.1 shows 1000 iterations of the logistic map with $r = 3.92$. The fixed point for this map is $x^* = 0, 0.7448$. In figure B.2, the histogram on top is obtained by using the exact Jacobian in the transformation. The histogram at the bottom uses the Jacobian obtained from the data set. Both histograms have a peak at $x = 0.745$.

B.2 Hénon Map

The Hénon map is often used to illustrate chaos in 2-D. One form of the mapping function \mathbf{F} for this map is:

$$\begin{pmatrix} x_{n+1} \\ y_{n+1} \end{pmatrix} = \mathbf{F}(x_n, y_n) = \begin{pmatrix} a + by_n - x_n^2 \\ x_n \end{pmatrix}.$$

The fixed points of the map \mathbf{F} can be obtained by setting $x_{n+1} = x_n = x^*$ and $y_{n+1} = y_n = y^*$ and then solve for x^* and y^* . The fixed points for the Hénon map are

$$x^* = y^* = \frac{-(1-b) \pm \sqrt{(1-b)^2 + 4a}}{2}.$$

For $a = 1.4$ and $b = 0.3$, the map is chaotic. Figure B.3 shows 5000 iterations of this map. The fixed points are $x^* = y^* = -1.5839$ and $x^* = y^* = 0.8839$. For this case, time delay coordinates were used to reconstruct the attractor. Figure B.4 is the result of the false nearest neighbor analysis and it shows that dimension 2 is required to reconstruct the attractor. Figure B.5 is the histograms of the transformed data set. The histogram fails to pick up the fixed point at $x^* = -1.5839$, but it does have a peak at 0.884. By inspecting figure B.3, it is clear that the point $x = y = -1.5839$ is not on the attractor. Repeated attempts to start the iteration with points close to $x = y = -1.5839$ show that even the first iteration will be far away from it. This leads to the conclusion that $x = y = -1.5839$ is an isolated fixed point. Any data set of the attractor shown in figure B.3 will not contain points close to the isolated fixed point. It is then impossible to pick up that fixed point using either the fixed point transformation method or the close return method.

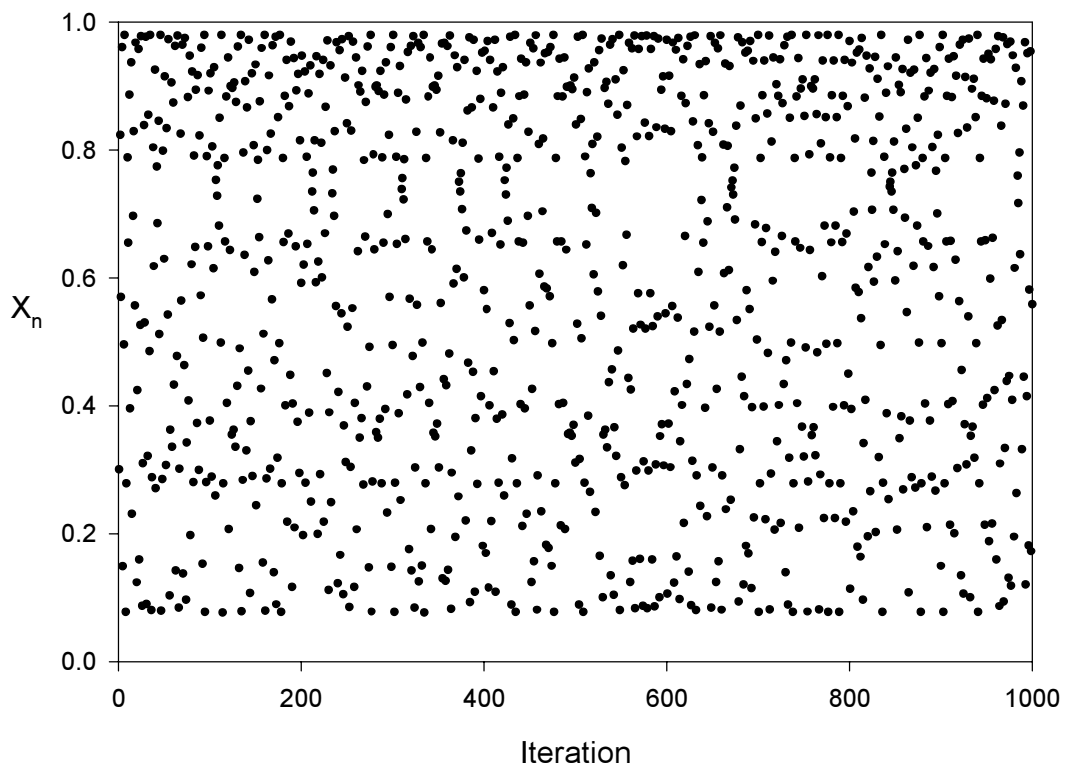


Figure B.1: 1000 Iterations of the Logistic Map

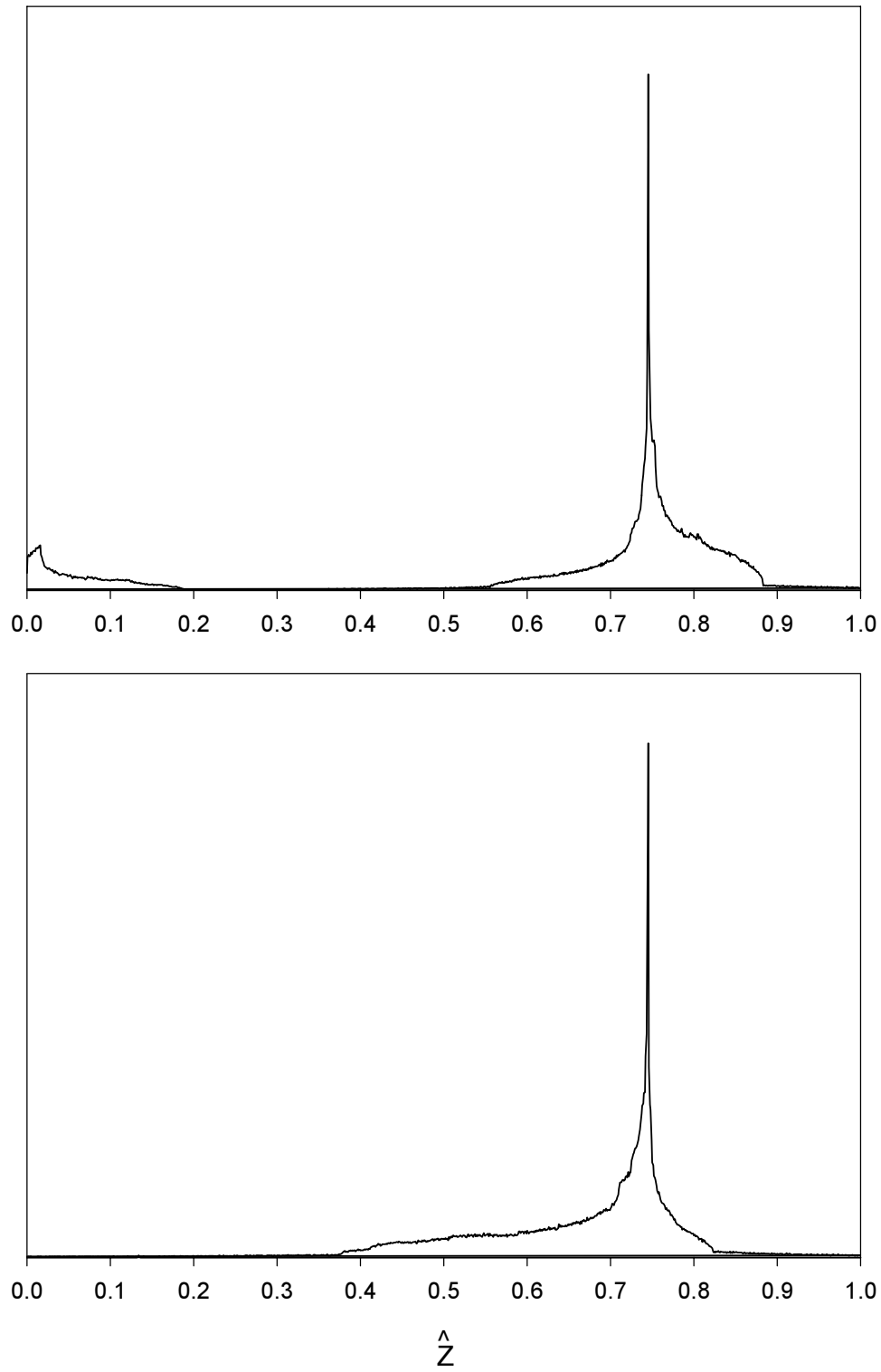


Figure B.2: The Histogram of the Transformed Logistic Map Data Set

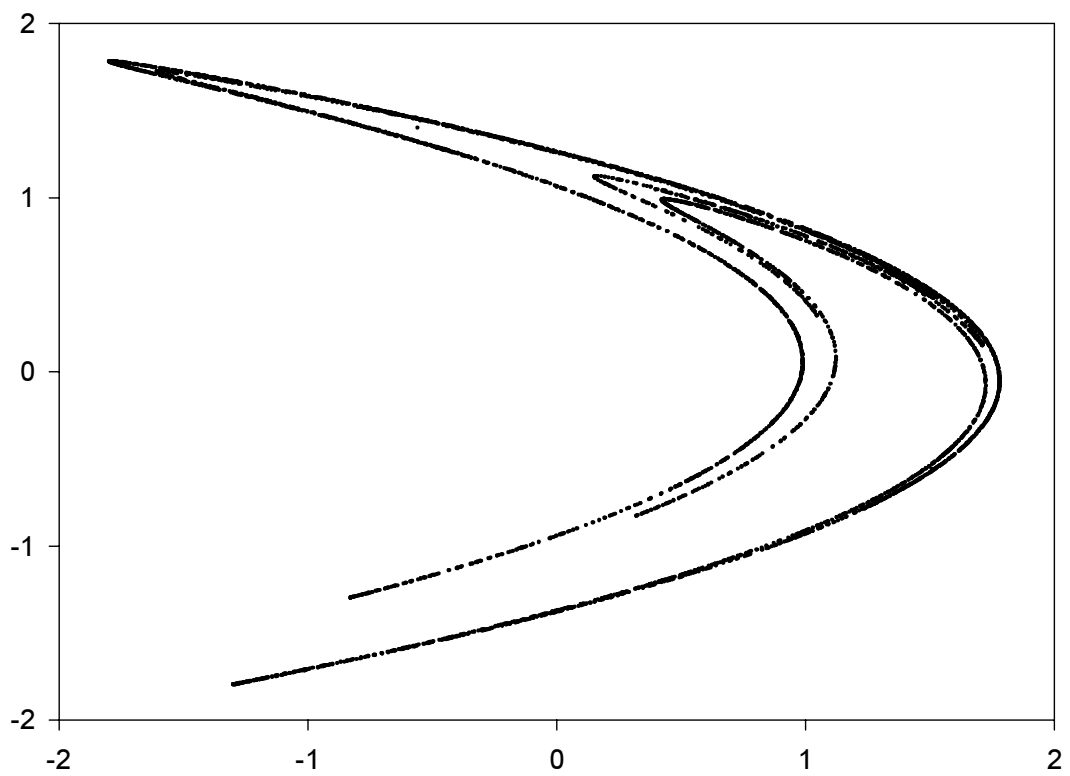


Figure B.3: 5000 Iterations of the Hénon Map

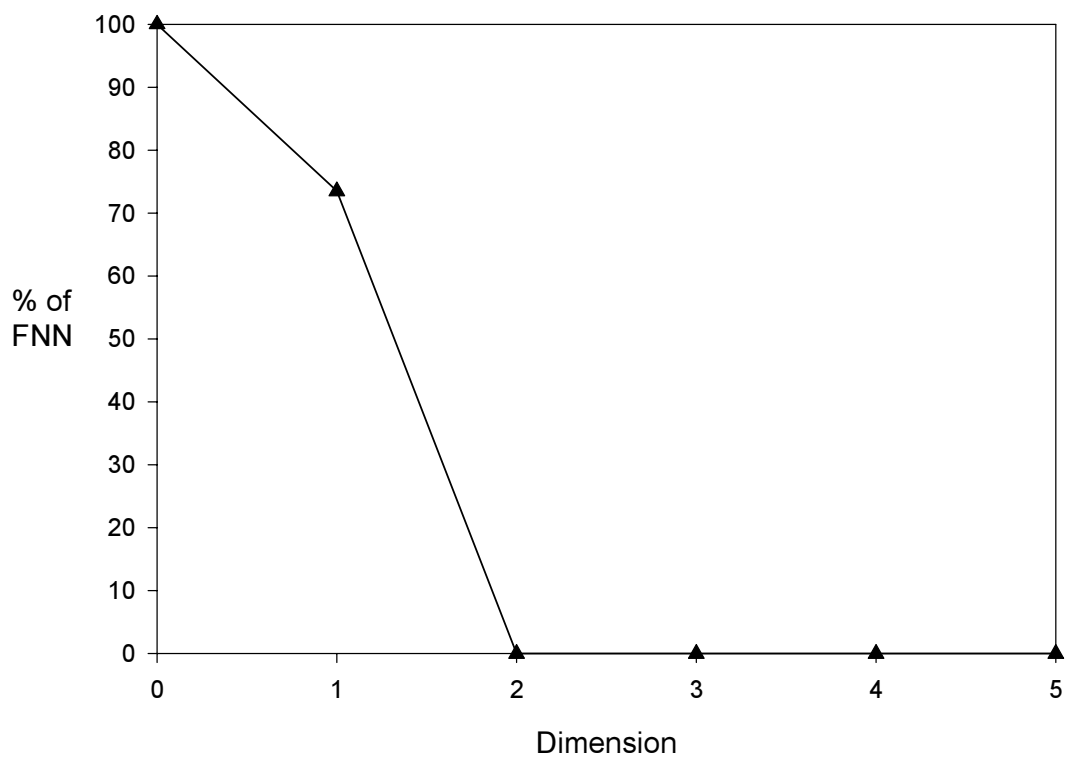


Figure B.4: False Nearest Neighbor Analysis for Hénon Map

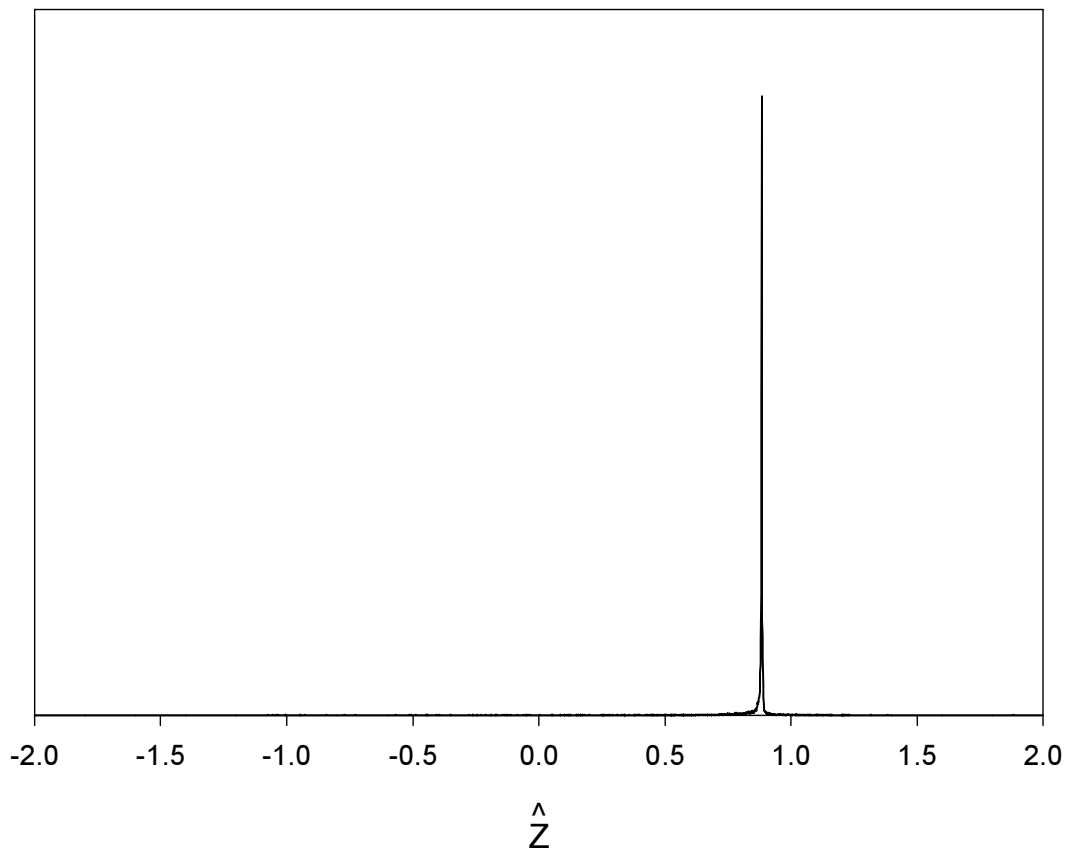


Figure B.5: The Histogram of the Tranformed Data Set for Hénon Map

Vita

Tseng-Hsing Hsu

Tseng-Hsing Hsu was born on March 17, 1963 in Miaoli, Taiwan. He attended National Taiwan University in 1981, studied Civil Engineering, and received his B. S. degree in 1985. From 1985 to 1987, he served in the army of the Republic of China.

In 1992, he received a M. S. degree from the department of Engineering Science and Mechanics of Virginia Polytechnic Institute and State University. After receiving the M. S. degree in Engineering Mechanics, he enrolled in the Ph. D. program at Virginia Polytechnic Institute and State University. After receiving his Ph. D. degree, he will go back to Taiwan and pursue a position in a research institute.